Lund University

Lund Institute of Technology
Department of Fire Safety Engineering

Flame Extensions Under Ceilings

Supervisor:
Prof. Nils Johansson

Candidate:
Martin Sturdy

Examiner:
Prof. Jonathan Wahlqvist

Master thesis submitted in the Erasmus Mundus Study Programme
International Master of Science in Fire Safety Engineering

Academic Year 2022-2023

DISCLAIMER

This thesis is submitted in partial fulfilment of the requirements for the degree of *The International Master of Science in Fire Safety Engineering (IMFSE)*. This thesis has never been submitted for any degree or examination to any other University/programme. The author(s) declare(s) that this thesis is original work except where stated. This declaration constitutes an assertion that full and accurate references and citations have been included for all material, directly included and indirectly contributing to the thesis. The author(s) gives (give) permission to make this master thesis available for consultation and to copy parts of this master thesis for personal use. In the case of any other use, the limitations of the copyright have to be respected, in particular with regard to the obligation to state expressly the source when quoting results from this master thesis. The thesis supervisor must be informed when data or results are used.

Read and approved,

Martin Sturdy

11/05/2023

Abstract

In this Master thesis project the factors affecting flame extension under flat and curved ceilings have been investigated. An experimental campaign was carried out in Lund University's Fire Lab using a propane gas burner and heptane pool fire in different positions and heat release rates within the setups. A flame recognition Python script was developed to identify the flame length in the videos taken for each test. The flame length data was then compared with flame length models found in the literature review. Results show that the flame extension under the curved ceiling were larger than under the flat ceiling: this is because the curved geometry affects the flow's buoyancy component, enhancing it and resulting in larger flames. Furthermore, the reduced entrainment of the side wall position makes unburnt fuel travel further under the ceiling extending the flame more. Differences in the flow characteristics also impacts the flame length: momentum driven flows such as that produced by the propane burner have a longer flame extension compared to the buoyancy driven flow of a pool fire. The greatest differences between the test data and the models found in literature result form the neglection of the flow's buoyancy component. Different test setups, fuels and test configurations can also be the cause of the found discrepancies. Adaptations of the relations put forward by the literature for the test results were therefore found in this work. Further study into different fuel types and burner positions would provide more information regarding the fire's behaviour beneath ceilings and keep structures and people inside them safe.

Abstract (IT)

In questa tesi magistrale sono stati studiati i fattori che influenzano l'estensione delle fiamme sotto soffitti piani e curvi. Una campagna sperimentale è stata condotta nel laboratorio dell'Università di Lund utilizzando un bruciatore a gas propano e un fuoco di eptano in diverse posizioni e usando diversi valori di potenza termica rilasciata all'interno delle configurazioni. È stato sviluppato uno script Python per il riconoscimento della fiamma e per identificare successivamente la lunghezza della fiamma nei video ripresi per ciascun test. I dati sulla lunghezza della fiamma sono stati quindi confrontati con i modelli trovati nella revisione della bibliografia. I risultati mostrano che l'estensione della fiamma sotto il soffitto curvo era maggiore che sotto il soffitto piatto: questo perché la geometria curva influisce sulla componente di moto ascensionale del flusso, potenziandola e determinando fiamme più grandi. Inoltre, il ridotto trascinamento che risulta nella posizione prossima alla parete laterale fa viaggiare ulteriormente il combustibile incombusto sotto il soffitto estendendo maggiormente la fiamma. Le differenze nelle caratteristiche del flusso influiscono anche sulla lunghezza della fiamma: i flussi guidati dalla quantità di moto come quello prodotto dal bruciatore a propano hanno un'estensione della fiamma più lunga rispetto al flusso guidato dal moto di ascensione tipico di un incendio di eptano. Le maggiori differenze tra i dati dai test e i modelli trovati in letteratura derivano dalla trascuratezza della componente di moto ascensionale del flusso. Diverse configurazione e carburanti utilizzati possono essere la causa di discrepanze

riscontrate. In questo lavoro le equazioni trovate nella biografia sono state adattate in base ai risultati trovati nei test. Ulteriori studi sui diversi tipi di combustibile e sulle posizioni dei bruciatori fornirebbero maggiori informazioni sul comportamento del fuoco sotto i soffitti e manterrebbero al sicuro le strutture e le persone al loro interno.

Acknowledgements

This section is dedicated to all the people that contributed and assisted me during this master thesis project.

I would like to deeply thank my supervisor Nils Johansson for the guidance, support and teachings throughout each step of this project. Thank you also to all the lab technicians that helped me setting up and performing the experimental campaign that was carried out during my thesis. Another thank you goes to St. Eriks for donating concrete pipes that made it possible to carry out the curved ceiling experiments.

The completion of this major milestone could not have been possible without the support of also several important people that I am privileged to have in my life. First and foremost I would like to thank all my family. My parents for the continuous selfless support and love that they have given me at every moment in my life; my brother for being close whenever needed; my grandparents and my aunt for making hard times easier. A special thank you goes to my girlfriend that has been my number one supporter when facing the challenges I have endured during this period. A big thanks goes to all my friends.

Contents

Chapter 1

Introduction

Fire safety engineering is an essential component in the design, construction and overall functioning of buildings, means of transportation and many other aspects of life. Its significance lies in the protection of life, the prevention of property damage, and the reduction of fire spread. Fire has been the main cause of many deadly and very serious incidents throughout history [1] and recent events have contributed to a more in depth study of the fire topic. In particular while the fire phenomena in itself is important, the design and analysis of fire protection systems and fire-resistant materials is critical to protect lives and properties. Therefore, the significance of Fire Safety Engineering lies in preserving the safety of the public and reducing the harm caused by fires.

One of the most important aspects of fire safety is the prevention of fire spread. Fire spread is the process of a fire expanding from its origin to other areas. As the fire grows, more heat and hot smoke are produced: the increasing heat flux can therefore promote ignition of nearby combustible objects and materials. The speed and range of the fire's spread depend on various conditions, such as the type of fuel, ventilation, and presence of protective measures. In order to protect the fire's sur-

roundings, knowledge regarding the mechanisms involved in fire development and ignition of nearby objects is necessary.

Flame extensions under ceilings are a particularly important aspect in Fire Safety Engineering since they have a direct impact on the fire spread and growth inside a compartment and to other parts of a building. In particular, if the ceiling is made of flammable material, spreading can occur sooner and can increase damage: this can cause the ceiling to collapse, compromising structural integrity and containment of the fire. The extension of flames are affected by different factors including compartment geometry [2] [3], ventilation [4], fuel type and fire size [5]. To prevent these problems, fire protection systems and fire resistant materials can be utilized: the spread of a fire can therefore be delayed, giving firefighters more time to respond and evacuate the building.

Typically, the geometry in most compartments is such that the ceiling is flat (horizontal): when a fire develops and grows, it can reach the ceiling creating a ceiling jet where flames extend horizontally beneath it. Nowadays, advances in architectural and building design see continuous innovation: this includes the utilization of curved structures, curved ceilings and structures such as tunnels. Extensive literature is present regarding tunnels [6], but not much focus is put into the flame extension aspect. For this reason, in this thesis the study of flame extensions under curved ceilings will be undertaken further and a comprehensive analysis of the various factors that contribute to their flame's behaviour in such settings will be conducted. Furthermore, a comparison with the same phenomena occurring under flat ceilings will be also outlined in order to provide greater knowledge regarding similarities and differences between the different ceiling geometries and their effect on flame extensions.

The remainder of this report is organised as follows. A comprehensive outline of the literature research procedure and results is presented in Chapter 2; Chapter 3 discusses the experimental setup and risks associated with the conducted fire tests; in Chapter 4 an explanation of the flame recognition software used to detect the flames from the fire tests is given; discussion of the test results is presented in Chapters 5, 6 and 7.

Objectives

In order extend the research on the topic of flame extensions under ceilings in this thesis some research objectives have been created and are outlined below:

1. Determination of models that have been developed to reproduce the behaviour of flame extensions under ceilings.

2. Determination of the impact of the ceiling structure (curved or flat) on flame extension under ceilings.

3. Determination of the effects of heat release rate (HRR), fuel type and burner location on flame extensions under ceilings.

4. Determination of the correlation between the test results and models and empirical correlations found in literature for flame extensions under ceilings.

The first objective will be answered by conducting a literature research, providing insights with regards to the methodologies used to predict flame lengths. The second and third objectives will be clarified by conducting the experimental

campaign throughout the thesis. Finally, the last objective will be achieved by comparing the literature review with the data and correlations that govern the flame extension phenomena.

Methodology

A literature review is the first step of this master thesis: in particular research on the state of the art of the *"Flame Extensions Under Ceilings"* topic will be conducted. This will give insight into what aspects of this topic have been evaluated and which have not; from this, a research area will be identified and focused on during the thesis. Literature on the fundamentals of confined fires propagation will also be reviewed. After having gathered information through the literature research, experimental setups will be created and the experimental campaign will be carried out. The data analysis is the final step of the project. Here, new data and information regarding "Flame Extensions Under Ceilings" will be analyzed and discussed to provide greater insight on this application. Test results will be compared to existing flame length models and adaptations of the existing correlations will be developed using linear regression. In this way, the existing work will be adapted further to consider how different burner positions, fuel types and ceiling geometry affect the flame length.

Chapter 2

Literature Review

In this chapter, a literature review on the topic of *"Flame Extensions Under Ceilings"* is undertaken. The goal of this part of the project is to understand what aspects of the topic have been already studied and identify research areas still to be examined. Furthermore, it is important to gain insight into the different models used to represent behaviour of flames and effect of different quantities on them when bounded by a ceiling. Finally, the literature review will also give insights into how experimental procedures have been undertaken: this will be important when setting up the experimental campaign and performing the tests in this project. Considering the importance of a clear and concise literature review, in this project an organised procedure was implemented and follows that of other publications in the literature [7].

2.1 Literature Research Methodology

The research procedure that has been followed for this project is summarized in the schematic in Figure 2.1. By following this methodology, the required information regarding existing literature related to the topic of *"Flame Extensions Under Ceilings"*

will be covered effectively and will be used to perform the work successfully.

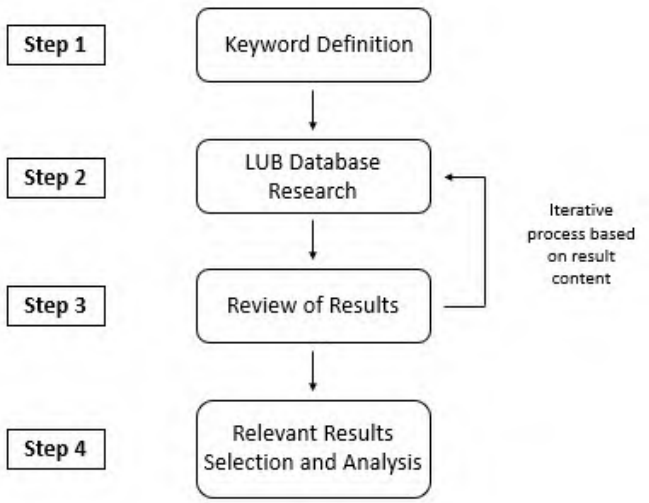

Figure 2.1: Literature Review Procedure

2.1.1 Keyword Definition

This first step of keyword definition is very important since keywords are essential in order to search for documents in databases: their combination, in fact, can help narrowing down relevant results within large collections of literature.

For this project, the keywords and their combinations were chosen based on their relevance and consultation between student and supervisor. The selected keywords are listed below:

- **Fire Flame* Extension* Under Ceiling***
- **Fire Flame* Length* Under Ceiling***
- **Flame* Ceiling* Jet**
- **Fire Jet Under Ceiling***
- **Flame* Ceiling* Surface***

- **Flame* Length Curved Ceiling***
- **Curved Ceiling* Jet**

The asterisk (*) symbol above certain keywords is used to include truncation in during the research and to narrow down results.

2.1.2 LUBSearch Database

After having identified the keywords and combinations, the second step of the literature review is to search for relevant papers in the *"Flame Extensions Under Ceilings"* topic. The LUBSearch site [8] of Lund University was used to perform the research. LUBSearch is a search engine where the university library's physical and electronic holdings can be accessed by users. The advanced search option consents to insert up to 5 keywords that can then be used in the exploration. Through the website, a significant portion of the Lund University Research Portal via SwePub is also available, as is the material of the library catalogue, LUBcat. LUBsearch incorporates Scopus and Web of Science: thanks to these, it is possible to find journal articles, websites, and conference proceedings. LUBSearch is therefore deemed an appropriate tool to use for the literature research and the results from the search process are regarded as adequate.

2.1.3 Review of Results

As shown in Figure 2.1, the third step is the revision of obtained results after the investigation with LUBSearch. Thanks to the precise definition of key words, 796 results were found for all seven keyword combinations outlined previously. The research produced on average 113 results per search. This shows once again that the selected keyword combinations are effective, concise and not too general.

After each of the seven searches, the results were analyzed initially by reading their titles. This was done to determine whether the results were relevant or not, therefore including or excluding them from further investigation; two examples for each the inclusion and exclusion processes are show below.

- **Inclusion**:

  1. ***Experimental*** *and theoretical analysis on* ***extension flame length*** *of buoyancy-induced fire plume beneath the* ***curved ceiling****.*
  2. *Effect of sidewall on the* ***flame extension characteristics beneath*** *a* ***ceiling*** *induced by carriage fire in a channel.*

  The titles of two results shown above were selected due to the inclusion of the words highlighted in bold. In particular these two titles include words such as *"Flame Length"*, *"Flame Extension"* that refer to the flame characteristics and *"Ceiling"* which is the part of the structure studied in this work. These also correspond with the keywords that were defined previously.

- **Exclusion**:

  1. *A study on the* ***maximum temperature*** *of ceiling jet induced by rectangular-source fires in a tunnel using* ***ceiling smoke extraction****.*
  2. *Flame extension lengths beneath a confined ceiling induced by fire in a channel with* ***longitudinal air flow****.*

  The titles of two results shown above were instead excluded from the search. *"Maximum temperature"*, *"smoke extraction"*, *"air flow"* are not quantities that have been analyzed in depth in this thesis. These words were not considered in the keyword selection either and have therefore been left out.

After filtering the research results, a total of 18 articles were chosen as relevant to the project.

2.1.4 Relevant Results Selection and Analysis

Following the review of results, the final stage of the literature review was undertaken. The 18 selected literature articles were read through thoroughly and relevant information used to further develop the project.

In particular, models used to describe flame characteristics and their spreading beneath curved and flat ceilings were noted and used in the project when applicable. Information regarding the experimental setup preparation and execution was also gathered while reading the relevant literature. Furthermore, in order not to miss any relevant information, relevant literature mentioned in the 18 selected papers was also investigated: this is referred to as the snowballing method [9].

2.2 Literature Overview

The topic of *Flame Extensions Under Ceilings* is important in the Fire Safety realm. In literature, the phenomena of Ceiling Jets and the fire's behaviour when reaching the ceiling has been studied in depth [10]. Here the work focuses mainly on the development of analytical and computational methods that represent the behaviour of such flows in terms of velocity and temperature. Further studies have supported these findings and extended their application to turbulent fires of different strengths [11] [12] and that develop under flat ceilings [13]. These results give important insight into the characteristics of such flows but do not deal with the length of flames.

Growth of fires in enclosures results in flames extending horizontally beneath the

ceiling. The flames can ignite objects and the heat transfer can reduce the time to ignition of the surroundings. In [14] correlations have been developed to establish flame length under a ceiling and the effect of both combustible and non-combustible ceiling linings on such extensions. The characteristics of the fire source are also important to determine its behaviour when impinging on the ceiling. In particular, axi-symmetric fires produce a radial flame area [5]; non axi-symmetrical fires (such as line-source fires) on the other hand produce flame lengths in two directions based on unburnt fuel mass flows distributed after impingement [15]. The flame extension area produced by the fire is a very important parameter that therefore needs to be considered: it significantly increases the heat flow towards the ceiling due to heat transfer region between the fire source and the ceiling [16]. This can cause problems with the stability of the building ceiling. The dynamics of the ceiling jet and the flame development for the different types of fires have been developed tanking into account the jet's entrainment and mixing rates [17].

The findings aforementioned deal with flat ceilings. Recently, similar studies have extended these issues to inclined and curved ceilings. With advances in architectural and building design, unique ceiling types are becoming more popular: curved ceiling structures such as tunnels are also gaining attractiveness in the urban infrastructure due to overpopulation problems and the consequent necessity to expand underground [18]. When flames from a fire develop in a compartment with a curved ceiling, the curved ceiling bends the flame shape [19]. The dependence of the flame's length on fire heat release rate and source-ceiling distance is of importance in these applications: in particular, higher heat release rate values increase the flame length and larger source-ceiling distances decrease the flame's extension [4]. These correlations result from experiments performed in curved ceiling tunnels: the increased flame length is caused by unburnt fuel and the variation of the buoyancy component

along the curved ceiling. Quantitative description of these phenomenons are given by models developed in literature [24].

The literature on *Flame Extensions Under Ceilings* gives valuable insight into the behaviour of fires in enclosures. For flat ceilings, extensive work has been developed on both the behaviour of the ceiling jet's flow and on the physical characteristics of the flames after impinging on the ceiling. You and Faeth performed using confined and unconfined fire tests to determine the flame extensions; Gao et Al. developed correlations to determine flame lengths when the fire is bounded by a sidewall; Zhang et Al. performed tests on inclined flat ceilings and created models for inclination angles between -20°and 20°. The flame extension phenomena for curved ceilings is less studied and further research is required to gain full understanding of the impact of this alternative ceiling geometry. Pan et Al. developed models for flame extensions under curved ceilings taking into consideration the changing buoyancy component of the flow induced by the curved geometry. These models will be explained and compared to the test results in the following chapters, extending the knowledge on flame extensions under curved ceilings and comparing it to the flat ceilings cases.

Chapter 3

Fire Characteristics

3.1 Flame Length

In this chapter a brief introduction on the theory behind flame length calculation is presented. The flame's length or height is the level at which the combustion process is complete [10]. During the combustion process, the hot gases produced are surrounded by the cooler air: since hot gases are less dense than colder ones, the density difference causes them to rise. This phenomena is referred to as buoyancy and is also responsible for the length flames can reach. In particular, if the fuel is not supplied at high velocities, buoyancy will dictate the upward velocity of the gaseous flow. Examples of buoyancy driven flows are those resulting from pool fires. On the other hand, if the fuel is injected at high velocities, the flow becomes momentum dominated and the buoyancy effect becomes negligible [30]. Jet flames are an example of momentum driven flows.

In literature extensive work has been performed to determine what properties influence the flame length [10] [30]. The Froude number derives from hydraulics but can be applied to the hot gases produced during combustion. It represents a relationship

between the flow velocity and buoyancy and is shown in the first term of Equation 3.1.

$$\mathrm{Fr} = \frac{\mathrm{v}^2}{\mathrm{g} \cdot \mathrm{D}} \propto \frac{\dot{\mathrm{Q}}^2}{\mathrm{D}^5} \tag{3.1}$$

The Froude number can also be related to the energy release rate, yielding the expression in the second term of Equation 3.1: D is the fuel source's characterisic diameter. Through experimental procedures, it was determined that the variation in flame geometry can be better represented with the square root of the Froude number (Equation 3.2).

$$\sqrt{\mathrm{Fr}} = \frac{\dot{\mathrm{Q}}}{\mathrm{D}^{5/2}} \tag{3.2}$$

$$\dot{\mathrm{Q}}^* = \frac{\dot{\mathrm{Q}}}{\rho_\infty \mathrm{c_p} \mathrm{T}_\infty \sqrt{\mathrm{gDD}^2}} \tag{3.3}$$

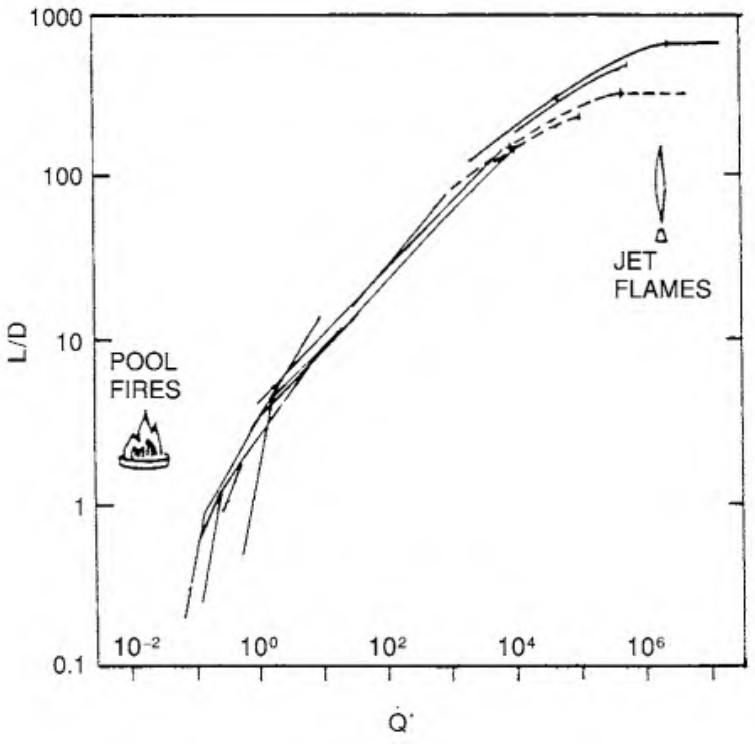

Figure 3.1: Comparison of normalized flame heights and HRRs obtained from literature [30].

Furthermore, by expressing the experimental data in terms of the non dimensional heat release rate, a new expression for the square root of the Froude number is obtained: this can be seen in Equation 3.3, where $\dot{Q}^*$ is the non dimensional HRR, $\dot{Q}$ is the fire's HRR, ρ_∞ is the density of air, c_p is the heat capacity of air and T_∞ is the ambient air temperature. In Figure 3.1, the numerous experiments undertaken to relate flame heights, energy release rates and fuel source diameter are shown. On the bottom left buoyancy dominated flows are represented while on the top right high momentum flows are shown. Extensive work performed by Heskestad [30] resulted in the creation of a correlation useful to represent the length of a fire's flame and is defined in Equation 5.2.

$$\frac{\mathrm{L_f}}{\mathrm{D}} = 0.235\dot{\mathrm{Q}}^{2/5} - 1.02 \tag{3.4}$$

This correlation is used to estimate the flame length of buoyant fire plumes and was developed from experimental data mostly using pool fires. In general, it is a rather simplified model since it assumes a steady-state, laminar, axisymmetric plume with no influence from external wind or turbulence. It was determined that the flame height is proportional to the square root of the heat release rate: for this reason, its application is not fully intended for for fires with flame heights that are significantly larger than the fuel diameter. Furthermore, while this equation is not intended for momentum driven flow fires, it can still provide a good estimation of the flame length. Heskestad's equation is not applicable for fires bounded by a wall or placed in a corner: in these cases, the geometry affects the combustion process, enhancing the HRR and extending the flame length [30]. To determine the flame length in cases where the fire is placed flush to a sidewall or in a corner, Equation 5.3 [38] can be used.

$$L_f = (1.681 - 0.005P)\left(0.235(\beta\dot{Q})^{2/5} - 1.02D\right) \tag{3.5}$$

where H_f is the total flame height of the wall bounded fire, β is the mirror coefficient that is a correction factor that accounts for the wall or corner bounding ($\beta = 1.6$ for wall fires, $\beta = 2.4$ for corner fires), P is the operating pressure value in kPa, Q is the heat release rate in kW and D the fire source diameter in meters. This equation is an adaptation of Heskestad's correlation but has been adapted to cases where the fire is bounded.

3.2 Heat Release Rate per Unit Area

Heat release rate per unit area (HRRPUA) is an interesting quantity that can be considered when determining the intensity of a fire: in particular, the higher the HRRPUA, the more intense the fire. It is defined in Equation 3.6 as the ratio between the heat release rate resulting from combustion and the area of the fuel source.

$$HRRPUA = \dot{Q}'' = \frac{\dot{Q}}{\mathrm{A}_f} \tag{3.6}$$

From the Equation above one can see that larger HRR and smaller A_f values cause the HRRPUA to increase. Based on this, a larger burner area does not necessarily result in a more intense fire. This is important to consider when testing different fuel types and flows that have different characteristics. Recalling the discussion on flame length from previously in the Chapter, jet flames and in general momentum driven fires tend to have larger HRRPUA values compared to buoyancy driven flows [10]. This will be important to consider when analyzing the results from the experimental campaign, which will follow in the next Chapters.

Chapter 4

Experimental Procedures

4.1 Experimental Setups

The comparison of flame extensions under curved and flat ceilings was undertaken utilizing two different setups. The flat ceiling setup was already present in the lab before the initiation of the experimental campaign; the curved ceiling setup instead was constructed especially for the thesis project.

4.1.1 Curved Ceiling Setup

The curved ceiling setup was constructed from scratch for this thesis project: two precast concrete pipes were utilized to create a tunnel like structure. Figure 4.1 illustrates a schematic of the setup including its dimensions. Each of the two concrete pipes had an internal diameter of 900mm, was 600mm long and 75mm thick. The weight of one pipe was of approximately 300kg and to put the two pipes together in order to form the complete structure, a crane was utilized. In literature, curved ceiling tunnel dimensions vary: in [22] two different tunnels were studied. Considering the cross section dimensions, the first tunnel had a width of 8.77m, height of

7.865m and 8.77m diameter corresponding to the curved ceiling; the second setup was larger measuring 11.89m in width, 10.66m in height and 11.89m in curved ceiling diameter. Comparing the setup used in this thesis to the dimensions found in literature, the scaling ratio is between 1:11 and 1:15 depending on which generic tunnel dimensions are taken as reference.

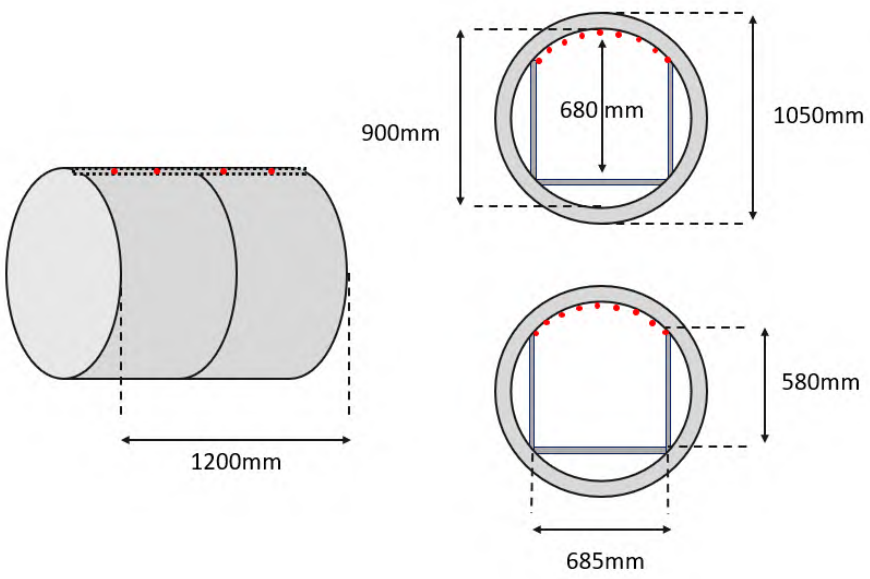

Figure 4.1: Schematic of the Curved Ceiling Setup

Once the two pipes were joined, the setup was secured in place with metal straps and placed on a Europallet to be moved with ease. Fire sealant [23] was applied on the top half of the setup in correspondence with the junction of the two pipes to ensure that fire and flames would not get out through the gap. Promatect H.ETA 06/0206 boards were used to create the structure inside the curved ceiling setup. These are high-performance boards used for passive fire protection applications. They are made of calcium silicate and is reinforced with selected cellulose fibers and fillers. The structure was fitted with three Promatect H.ETA 06/0206 boards to form the sidewalls and floor of the tunnel setup: this can be seen in the cross section schematic of Figure 4.1. In order to measure temperatures in the curved

ceiling setup, 13 K-type thermocouples were used: 9 were placed at the centre of the configuration along the cross-section each 10cm from each other, while the remaining four were placed longitudinally across its length and with 25cm separation form each other. In total, considering the thermocouple positioned in the middle of the cross section, the longitudinally placed thermocouples are 5.

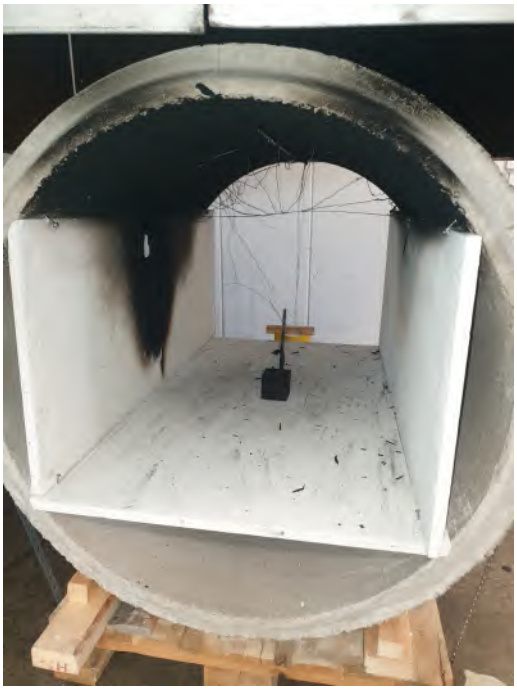

Figure 4.2: Curved ceiling setup

In Figure 4.2 the previously mentioned features of the curved ceiling setup can be seen: the metal wire structure used to hold the thermocouples in place can also be seen on the ceiling of the setup.

4.1.2 Flat Ceiling Setup

The second setup used to test the flame extension under flat ceiling was already present in the laboratory. It was originally utilized as a 1/3 scale ISO 9705 room during previous experiments in the lab. The back side of the flat ceiling configuration

could be opened making it a rectangular cross section tunnel like structure for the experiments in this thesis project: its schematic is shown in Figure 4.3. The second side was partially open. The floor was raised by 10cm in order to have the same centreline height as in the curved ceiling setup. The board used for the setup's floor was a Promatect H.ETA 06/0206 [25] board. In literature, rectangular cross section tunnels typically have a width of 9m and height of 6m [21]. The flat ceiling setup used for the tests therefore approximately represents a 1:11 scale model.

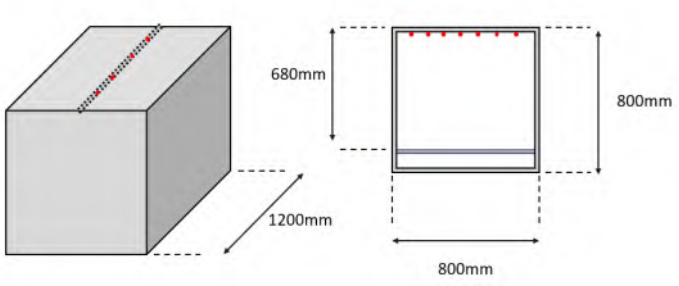

Figure 4.3: Schematic of the Flat Ceiling Setup.

In Figure 4.4 below, the flat ceiling setup can be seen. In order to measure temperatures inside the setup and to evaluate the flame's position, K-type thermocouples were also installed: these are identified by the red dots in Figure 4.3. Overall 7 thermocouples distanced 10cm from each other were placed across the centre of the structure's cross-section; four additional thermocouples were installed longitudinally with 25cm between them. As for the curved ceiling setup, considering the thermocuple placed in the centre of the cross section of the flat ceiling configuration, the longitudinally placed thermocouples become 5. These can be seen in Figure 4.4 alongside the raised floor and the partially opened side.

Figure 4.4: Flat Ceiling Setup.

4.2 Fuel and Burner Characteristics

In the previous Section, the two different ceiling setups have been described. While the ceiling's geometry is one of the parameters that have been varied in order to determine the difference in the flame extensions, also two fuel types have been utilized. Specifically, heptane and propane have been used in the tests: Table 4.1 outlines some physical characteristics of the fuels that were utilized.

Fuel	**Physical State at 25°C**	**Composition**	**Heat of Combustion [MJ/kg]**
Propane	Gas	C_7H_{16}	44.56
Heptane	Liquid	C_3H_8	46.45

Table 4.1: Characteristics of the fuels used in the experimental campaign [10].

Propane was burned through a square sandbox burner measuring 0.074x0.074m: the burner was connected to the gas supply line through a pipe and the gas flow rate could be controlled thanks to an electronic flow meter. By adjusting the flow outputted by the flow meter, different HRR values could be tested. The ignition of the gas was performed utilizing a live flame and by opening the gas flow tap. For heptane, a pool fire was utilized: a square metal vessel measuring 0.18x0.18m was used in this case. In order to have an even surface for the heptane to burn on, a portion of water was placed inside the vessel. Since heptane does not mix with water and its density is lower than the water's, the fuel floats on the surface and could be easily ignited using a live flame. Extensive studies have determined that the HRR and burning rate of pool fires depend on several parameters [30]: one of these is the diameter of the pool, hence for the experiments utilizing this fuel type, the HRR could not be varied like in the case of propane. In the following Section 4.4, the different tests that were performed have been outlined.

4.3 Data Collection

The experiments that were carried out for this project were undertaken in the fire lab under a smoke extraction hood. This was done both to extract the hot smoke from the premises for safety reasons and to analyze the gases. Figure 4.5 shows the experimental setup and the extraction hood which was connected to a duct measuring 20cm in diameter. The hood is equipped with various equipment such as a fan for different levels of extraction in the duct, a bi-directional probe for dynamic pressure difference measurements, a light source and photocell for optical density detection, thermocouple for temperature measurements. At intervals of 1 second, the gases are extracted and analyzed: in addition to the quantities mentioned above, oxygen, carbon monoxide and carbon dioxide measurements are also performed.

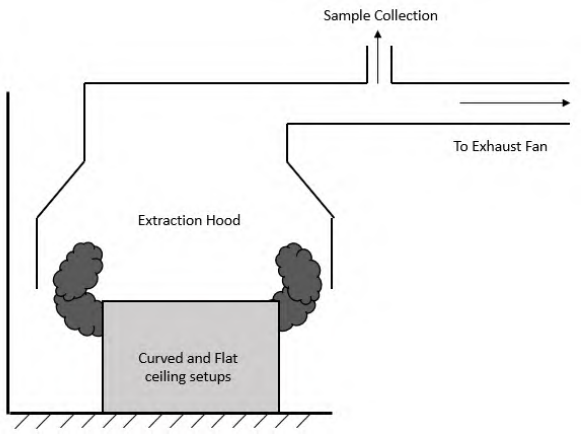

Figure 4.5: Schematic of the flat and curved ceiling setup positioning in the lab and extraction hood placement.

Analysis of the gases is important because thanks to the concentration values of O_2, CO_2 and CO the heat release rate obtained during the tests can be calculated. It has been determined that the heat released per unit of oxygen consumed is constant: this can be used to determine the heat release rate of a combustion process. Furthermore, accuracy of these calculations can be improved by measuring the variation of CO_2 and CO concentrations during the process. Equations have been developed to calculate the HRR looking at the variation of these quantities [33]. The HRR and other values that are measured in the hood are useful to understand the phenomena occurring during the combustion process and will be utilized in the discussions presented in subsequent sections.

4.4 Performed Tests

Previous sections outlined two of the parameters that were varied in the different tests to investigate their effect on flame extensions under ceilings. This section outlines all the tests that were performed throughout the experimental campaign. Alongside the variation of ceiling geometry and fuel type, also the heat release rate

of the fires and their location within the different setups were studied. The HRRs for the propane burner could be changed by varying the gas flow rate; the heptane had a fixed HRR. The tests performed in the lab are outlined in Table 4.2.

Equation 4.1 can be used to estimate the theoretical heat release rate for the heptane pool fire:

$$\dot{\mathrm{Q}} = \mathrm{A_f}\dot{\mathrm{m}}''\chi\Delta\mathrm{H_c} = 25kW \tag{4.1}$$

Where A_f is the area of the pool, $\dot{\mathrm{m}}''$ defined in Equation 4.2 is the free burn mass loss rate , $\chi = 97\%$ [31] is the combustion efficiency of heptane and $\Delta\mathrm{H_c} = 44.45MJ/kg$ [30] is the heat of combustion of heptane.

$$\dot{\mathrm{m}}'' = \dot{\mathrm{m}}''_{\infty} \cdot \left(1 - \mathrm{e}^{-\mathrm{k}\beta\mathrm{D}}\right) \tag{4.2}$$

For heptane $\dot{\mathrm{m}}''_{\infty} = 0.101$ and $k\beta = 1.1$ [30].
For propane, four flow rates were tested in order to obtain smaller and larger fires. For this fuel, Equation 4.3 was utilized to obtain the HRR value from the different gas flow rates. Here, $\dot{V}$ is the gas flow rate in m^3/s, $\rho_g = 1.8kg/m^3$ [32] is the density of propane at ambient temperature, $\Delta H_c = 44.56MJ/kg$ [30] is the heat of combustion of propane and $\chi = 95\%$ [10] is the combustion efficiency. For the four gas flow rates of 0.30, 0.40, 0.50 and 0.75 L/s, the corresponding heat release rates result to be 23.90, 31.91, 39.90 and 59.83 kW respectively.

$$\dot{Q} = \dot{V} \cdot \rho_g \cdot \Delta H_c \cdot \chi \tag{4.3}$$

The effect of different burner positions inside the tunnel was also investigated: the burners were placed in a central and side position (flush to one of the walls) in the different tests. Below, in Figures 4.6 and 4.7, the placement of the burner

positions for the flat ceiling setup and the distance to the ceiling in meters is shown in the figures. In all tests performed with the heptane pool, a set of bricks was placed under the heptane vessel to ensure the fire impinged the ceiling. For the flat ceiling setup, also an elevated case made with an additional pair of bricks was tested.

Run	**n. Tests**	**Fuel**	**Ceiling Type**	**Position**	**Gas Flow Rate/HRR**
1	3	Propane	Flat	Centre	0.3L/s
2	3	Propane	Flat	Centre	0.4L/s
3	3	Propane	Flat	Centre	0.5L/s
4	3	Propane	Flat	Centre	0.75L/s
5	3	Propane	Flat	Side	0.3L/s
6	3	Propane	Flat	Side	0.4L/s
7	3	Propane	Flat	Side	0.5L/s
8	3	Propane	Flat	Side	0.75L/s
9	3	Propane	Curved	Centre	0.3L/s
10	3	Propane	Curved	Centre	0.4L/s
11	3	Propane	Curved	Centre	0.5L/s
12	3	Propane	Curved	Centre	0.75L/s
13	3	Propane	Curved	Side	0.3L/s
14	3	Propane	Curved	Side	0.4L/s
15	3	Propane	Curved	Side	0.5L/s
16	3	Propane	Curved	Side	0.75L/s
17	3	Heptane	Flat	Centre	25kW
18	3	Heptane	Flat	Centre-Elevated	25kW
19	3	Heptane	Flat	Side	25kW
20	3	Heptane	Flat	Side-Elevated	25kW
21	3	Heptane	Curved	Centre	25kW
22	3	Heptane	Curved	Centre-Elevated	25kW
23	3	Heptane	Curved	Side	25kW
24	3	Heptane	Curved	Side-Elevated	25kW

Table 4.2: Experimental test list

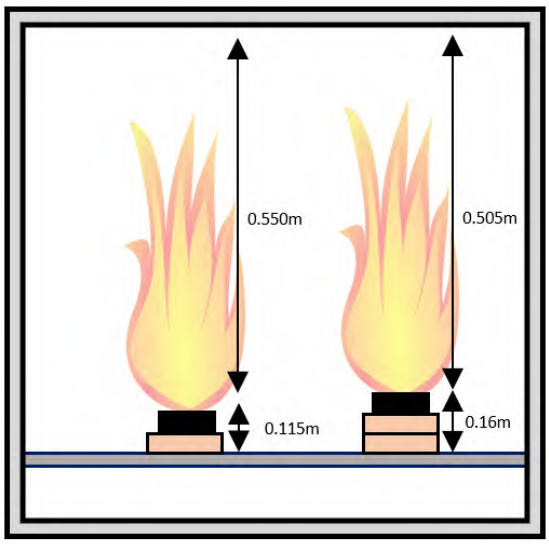

Figure 4.6: Schematic of heptane pool position and heights to ceiling in the flat setup

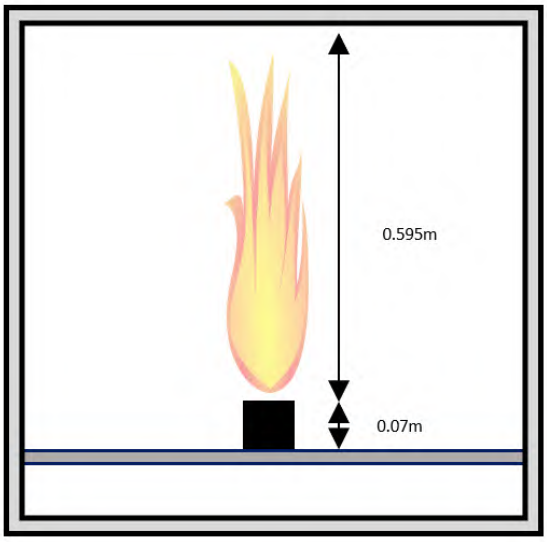

Figure 4.7: Schematic of propane pool position and heights to ceiling in the flat setup

Similarly, the heights and burner positions are also shown for the curved ceiling case in Figure 4.8 and Figure 4.9.

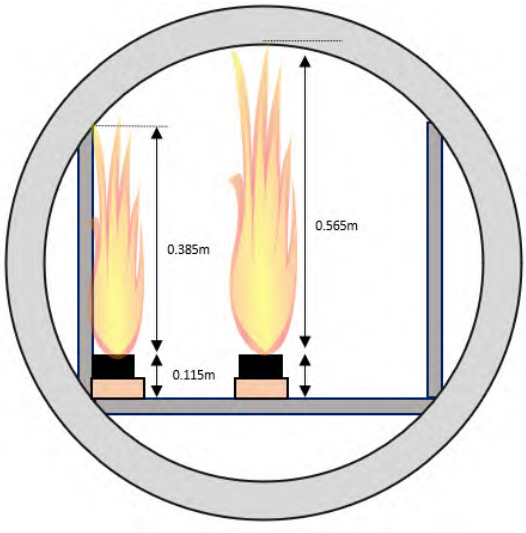

Figure 4.8: Schematic of heptane pool position and heights to ceiling in the tunnel setup

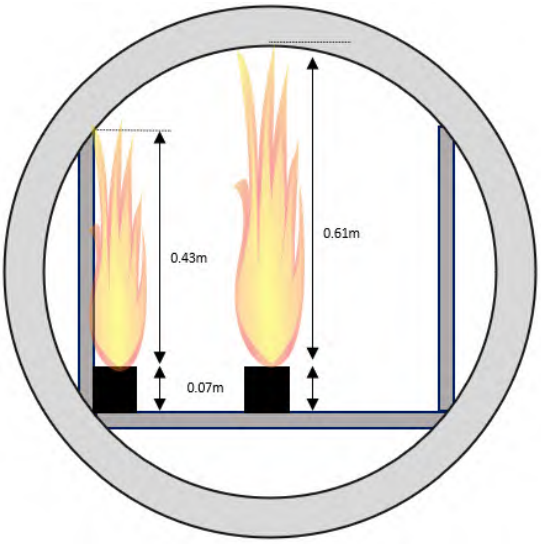

Figure 4.9: Schematic of propane pool position and heights to ceiling in the tunnel setup

Finally, in order to obtain good accuracy, reliability and for averaging of the results, each test was repeated 3 times.

4.5 Risk Analysis

The practical part of the thesis project on the topic of *"Flame Extensions Under Ceilings"* consists in executing fire tests in Lund University's fire lab. In order to carry out the fire tests in a safe manner during the experimental campaign, a risk analysis has been carried out to identify hazards related to such activities. In addition to the risk analysis, a lab test document has been submitted to relevant parties before the experimental procedures were carried out: in this document, the policies regarding safety, handling of flammable substances, disposal of materials and more have been discussed in accordance with the relevant documentation that describes these operations [26] [27] [28] [29]. During the test it is expected that a minimum of 2 people will be present in the lab: this includes the student carrying out the tests, an assistant, one or more lab supervisors and potentially other students working in the lab or lab visitors. Before the initiation of the lab sessions, safety review and review of laboratory elements is carried out by a lab supervisor.

	Risk Identification
1	Liquid fuel ignition resulting from spillage. Refilling of recently used hot vessels is also performed.
2	Gaseous fuel fire resulting from ignition of overflowed gas.
3	Presence of smoke in the lab resulting from too large a fire and inadequate fan extraction capacity.
4	Fire too large reaching the hood containing the extraction system and fan.
5	Smoke inhalation and burns. Temperature measurements of flames need to be performed and there is risk to be too close to the flame. Burns may also occur when handling hot vessels and burners.
6	Contact with harmful chemicals: heptane and propane are utilized as fuels.
7	Fire spread to other materials or objects.
8	Handling of heavy experimental setups: heavy concrete structures are used and need to be handled with caution.

Table 4.3: Risk Identification for the experimental setup of the project.

Table 4.3 outlines the risks that may be faced when carrying out the tests in the lab. Table 4.4 then explains the safety measures that will be utilized to reduce the risks stated in the risk identification matrix.

	Risk and Mitigation Measures
1	Unattentive handling of the fuels and of the vessels used to contain them can result in spillage. The filling of the vessels must be done with caution and should not be performed when such vessels are heated (for example just after being used). Information is provided before the beginning of the experiments.
2	Knowledge regarding how gas may be ignited is given prior to the experiments. Functioning of the gas tap is instructed before use by lab supervisors.
3	The rate of the fans in the extraction system needs to be adequate for the tested fire size. One experiment at a time is conducted. Lab supervisors may monitor and adjust the fan speed. Interruption of the experiments and ventilation of the lab must be performed if smoke overflows from the hood and enters the lab room.
4	For liquid fuels, the vessel with 30cm in diameter must be utilized. For the gas burner, the HRR must not exceed 60kW of power.
5	Information regarding the correct procedures and associated risks is given prior to the experiments. Lab supervisors should be present when critical procedures are carried out to ensure safety. People with long hair should have it tied up. The handling of vessels and burners should be performed using protective gloves. Security glasses should be worn. Only the person igniting the fuel should stand close to the vessel or burner.
6	The handling of liquid fuels must be monitored by the lab supervisor. The refilling of the vessels must be performed close to the fire testing site. Protective glasses and gloves should be worn when performing such tasks. Interaction with the gaseous fuels should only be done when performing ignition.
7	Material of combustible nature that has not to do with the experiments must not be present under the hood. Any combustible material should be placed at a minimum of 1.0m horizontally from the hood to avoid ignition. The control tap for the gas burner should be placed in the off position when experiments are not performed.
8	Caution must be used when dealing with the experimental setups. The weight of the setups can reach 600kg and injuries may occur if mishandling occurs. The setup should be safely secured to the structure used to move it.

Table 4.4: Risk and Mitigation measures for the experimental setup of the project.

In Table 4.5, the risk and mitigation measures from Table 4.4 are placed in a

Risk Matrix. Here the different colours represent the risk levels. In particular:

- Green: the identified risk is mitigated thanks to the measures put into place in the lab.
- Yellow: the risk is reduced through the mitigation measures, but needs to be monitored.
- Red: the risk is not mitigated and actions need to be put in place to reduce it.

Risk Matrix		Probability				
		Unlikely	**Rare**	**Possible**	**Likely**	**Very Likely**
Consequence	**Negligible**		**3, 4**			
	Small	**6**	**1, 5, 8**			
	Medium	**7**	**2**			
	Large					
	Disastrous					

Table 4.5: Risk Matrix for the experimental setup of the project.

Chapter 5

Heat Release Rates and Determination of Flame Extensions

5.1 Heat Release Rates

Using the varying concentrations of O_2, CO_2 and CO from the hood measurements and using the Equations put forward in literature [33], the heat release rates of the tests could be calculated. Chapter 4 also described the burner and fuel characteristics and how the theoretical HRRs were calculated. Table 5.1 summarizes the theoretical HRRs alongside the values found from the analysis of the hood gases. From the table it is clear that the HRR values measured during the tests are significantly different from the ones found using the theoretical expressions. The differences can be attributed to several factors. The expressions used to calculate the theoretical heat release values are limited since they provide a value that depends only on the chemical characteristics of the fuels and parameters such as gas flow and fire source diameter. On the other hand, they do not account for external factors that also

play a role in the combustion process. Namely, the geometry of the structures can have an effect on the rate of combustion of each fuel source, reducing or enhancing it. This is particularly valid for the heptane pool, since for the propane case, the flow is set through the flow meter.

Fuel/Position	**Measured HRR [kW]**
Propane - Flat, Centre	40.1, 50.8, 62.1, 94.2
Propane - Flat, Side	42.3, 53.4, 65.2, 96.2
Propane - Tunnel, Centre	40.7, 52.4, 63.9, 100.9
Propane - Tunnel, Side	40.8, 51.3, 63.8, 100.5
Heptane - Flat, Centre (Elevated)	59.9, (80.4)
Heptane - Flat, Side (Elevated)	48.7, (69.6)
Heptane - Tunnel, Centre	61.6
Heptane - Tunnel. Side	49.2

Table 5.1: Theoretical and measured HRR values for the performed tests.

Furthermore, malfunctioning of equipment could also play a role in the differences seen in Table 5.1. The propane gas flow system had a small leak that made a small quantity of gas flow when the tap was opened: this would have an effect on the overall HRR, which can explain the differences seen above.

The complete heat release curves obtained from the heptane tests in the two different setups are shown in Figure 5.1. The shape of the curves is similar between each other and follows the expected bell pattern. After ignition the heat release rate begins to rise and, as the combustion reaches a steady state, we have a period where the HRR can be considered as constant (the top part of the curves). After the steady state, as the fuel begins to run out, the heat release rate values start to reduce until the fuel finishes. The maximum HRR values are different between the tests but a general pattern can be seen. The side configurations generally have a lower HRR value compared to the centre cases: when the pool is flush to the side

walls of the setups, the entrainment is reduced resulting in a lower mass loss rate (MLR) and consequently lowering the HRR as can be seen in Equation 4.1.

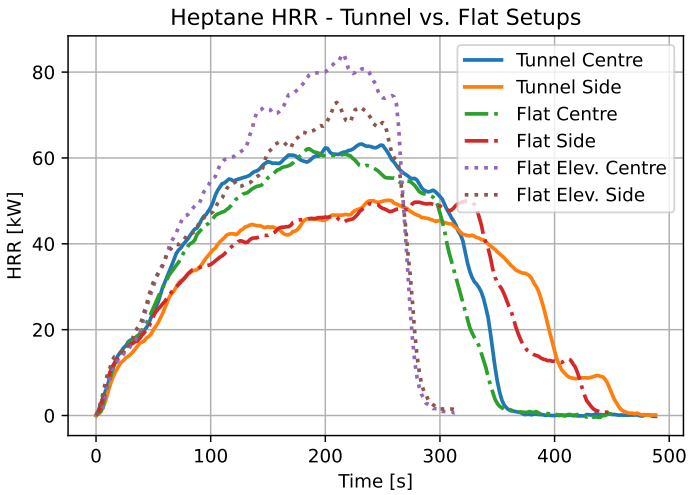

Figure 5.1: HRR values for the Heptane tests.

As mentioned in Chapter 4 when describing the experimental setups, for the flat ceiling case the pool was elevated further to estimate the effect of the height variation. In Figure 5.1, the heat release rate corresponding to the elevated scenario is depicted by the dotted curves. Similarly to the other data, the heat release rate of the side position is lower than the centre one confirming that the reduced entrainment reduces the HRR. Both cases though have a higher maximum heat release rate compared to the non-elevated cases. With the additional elevation, the flames impinged the ceiling significantly more: the radiative feedback from the ceiling increases the rate of combustion [34] of the fuel and consequently the MLR. Referring once again to Equation 4.1, the increased MLR results in an increase in heat release rate. The increase in rate of combustion can also be noticed from the reduced time the heptane takes to burn, resulting in a narrower bell shaped curve in Figure 5.1.

Figure 5.2: Heptane Flat Centre

Figure 5.3: Heptane Flat Side

Figure 5.4: Heptane Tunnel Centre

Figure 5.5: Heptane Flat Centre Elevated

Figure 5.6: Heptane Flat Side Elevated

Figure 5.7: Heptane Tunnel Side

Figures 5.2 through 5.7 show the fires for the heptane tests. As just discussed, it can be seen how for the elevated setups in Figures 5.5 and 5.6 the ceiling is much closer and how the radiative feedback can influence the burning rate.

Results from the propane tests are shown in Table 5.1. Here, the four different flow rates that were tested can be seen: overall, the HRR values are similar for each case. Pictures of the propane tests with the flat ceiling setup can be seen in Figures 5.8 to 5.15: one can see how the fire becomes more intense and the flame extension under the ceiling increases as the flow rate increases. With the higher flow rates, the flames also extrude from the setup as shown in Figures 5.14 and 5.15.

Figure 5.8: Propane Flat Centre - 0.3L/s

Figure 5.9: Propane Flat Centre - 0.4L/s

Figure 5.10: Propane Flat Centre - 0.5L/s

Figure 5.11: Propane Flat Side - 0.3L/s

Figure 5.12: Propane Flat side - 0.4L/s

Figure 5.13: Propane Flat Side - 0.5L/s

Figure 5.14: Propane Flat Centre - 0.75L/s

Figure 5.15: Propane Flat Side - 0.75L/s

For the curved ceiling setup, Figures 5.16 to 5.23 show the fire's evolution with the gas flow rate variation. Similarly to the results that can be seen for the flat ceiling case, the higher the flow rate, the more intense the fire and the longer the flame extension under the ceiling. Visually, one can also see how for the curved ceiling case the flame appears to extend more compared to the flat ceiling case for the same gas flow rate. This is particularly evident for the tests where the burner is placed flush to the tunnel sidewall.

Figure 5.16: Propane Tunnel Centre - 0.3L/s

Figure 5.17: Propane Tunnel Centre - 0.4L/s

Figure 5.18: Propane Tunnel Centre - 0.5L/s

Figure 5.19: Propane Tunnel Side - 0.3L/s

Figure 5.20: Propane Tunnel side - 0.4L/s

Figure 5.21: Propane Tunnel Side - 0.5L/s

Figure 5.22: Propane Tunnel Centre - 0.75L/s

Figure 5.23: Propane Tunnel Side - 0.75L/s

A final interesting parameter to consider knowing the maximum heat release rate values obtained in the tests and the burner area for each fuel type, is the heat release rate per unit area (HRRPUA). As mentioned in Chapter 3, this quantity differs for buoyancy and momentum driven flows. Table 5.2 shows the average HRRPUA values for the two fuel types. In the tests the burners both have a square geometry where the heptane pool's side measures 0.18m and the propane burner's side measures 0.074m.

Fuel	Burner Area [m2]	Average HRR [kW]	Average HRRPUA [kW/m2]]
Propane	0.005476	40.9, 51.9, 63.8, 97.9	7468.9, 9477.7, 11650.8, 17878.0
Heptane (Elevated)	0.0324 (0.0324)	61.6 (80.4)	1901.2 (2481.5)

Table 5.2: HRRPUA for the different fuels.

It is clear that the intensity of the fire produced by the propane burner is much higher than that of heptane. This is expected since the propane fire is a momentum driven flow: additionally, the HRR values tested are higher than the heptane test ones. Furthermore, since the propane burner area is smaller than the heptane's one, the HRRPUA is expected to be higher. These results are important to consider for later Chapters when the analysis of the results found for the flame extension beneath the ceiling will be discussed.

5.2 Video Analysis Code

In order to measure the length of the flame extensions under the flat and curved ceilings, an ad-hoc image analysis script was created. The coding of such a script was done using the Python programming language and implementing the Open CV library [35]. Open CV (Open Source Computer Vision Library) is an open source computer vision and machine learning software library: amongst many other libraries, Open CV has an advanced computer vision library. Thanks to the unique features of the library and the versatility of the Python coding language, a code capable of detecting fire in videos and images was produced for this thesis. The code is found in Appendix A. Throughout the experimental campaign, for each test a set of pictures, normal and slow-motion videos were taken in order to measure the flame extension under the ceilings using the fire detection Python script. A "Samsung Galaxy S9+" smartphone's camera was utilized to take the videos and photos of the experiments. It's has a 12 Megapixels camera and the normal speed

videos were recorded at 1080p definition with 30 frames per second (FPS); for the slow-motion videos, the recording definition was also set at 1080p, but the recording was performed at 240 FPS.

The basic principle behind the functioning of the code and its ability to identify fire is pixel identification. The code was implemented in the "Google Colab" [36]environment, an online Python compiler. Below, the steps followed by the code to perform the video analysis are outlined:

- **File Upload:** The videos are uploaded to the Colab local file storage. The videos files all had an .mp4 format.
- **Video Information:** Information on the video file is then obtained utilizing specific commands from Open CV. In particular, the frame count, FPS, height and width of the video's frames is taken. During the recording of the videos, it was ensured that the frame height corresponded with the free height of the setups: this was very important in order to obtain the pixel to meter relationship required to calculate the flame length in subsequent steps in the code.
- **Output Video File Creation:** An .mp4 file is created, with the same characteristics as the input video files, to output the processed video frames.
- **Fire Recognition:** A loop is initiated in the code to run through each frame of the inputted videos until no more frame is found. Once each frame is extracted, its pixels' colours are converted from RGB (Red Green Blue colors) to HSV (Hue Saturation Value): this step is performed to ease the pixel colour detection since with HSV colour variations can be detected better. A mask was then defined to identify the fire pixels that fell in the desired colour range

defined beforehand in RGB colors: the range for the video analysis performed went from (255, 170, 40) corresponding to a light orange to (255,0,0) corresponding to red. Using the mask, the fire pixels are extracted and only the flame is visible. An example of the result obtained from the video analysis can be seen in Figure 5.24

Figure 5.24: Result of the video analysis performed on the experiment's video recordings.

- **Bounding Rectangle Creation:** After having detected the fire, a bounding rectangle code was created in order to measure the flame's length. The bounding rectangle uses the Cartesian coordinates from the Python code to highlight the fire pixels: an example of the results obtained from this part of the code can be seen in Figures 5.25 and 5.26. In the figures, it is clear how the bounding rectangle surrounds the whole area of the fire. The rectangle's dimensions in pixels are then saved for each frame and converted to meters using the ceiling's free height and frame height: since the ceiling's free height in meters and the frame's height in pixels were both known, the pixel to meter ratio could be found and applied to the flame length. In particular, the bounding rectangle's width was taken as the flame extension length. For the flat ceiling case, the width could be used directly; for the curved ceiling the curved flame extension needed to be calculated from the width value using

Figure 5.25: Results from the bounding rectangle for heptane in the flat ceiling setup.

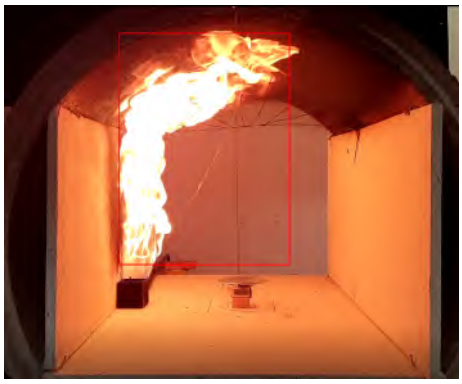

Figure 5.26: Results from the bounding rectangle for propane in the curved ceiling setup

trigonometry and arc geometry using Equation 5.1.

In the equation, r_up is the arc length, d is the distance from the tunnel's center line and R is the radius of the tunnel.

$$r = R \arcsin \frac{d}{R} \tag{5.1}$$

Since each test was performed three times in order to minimize errors, a multitude of videos were recorded and analyzed. In Figure 5.27, an example of the flame video analysis results processing is shown. For each test, analysis of both the normal and slow motion videos was performed: information of the bounding rectangle's width and height were saved in an Excel file and averaged. This was performed for each of the three tests. The average was then taken of the three tests to have a final averaged value for both the width and height of the bounding rectangle: for the flame length calculations, only the rectangle's width was taken, as explained previously. The same procedure was followed for all tests with the different setups and different fuel types.

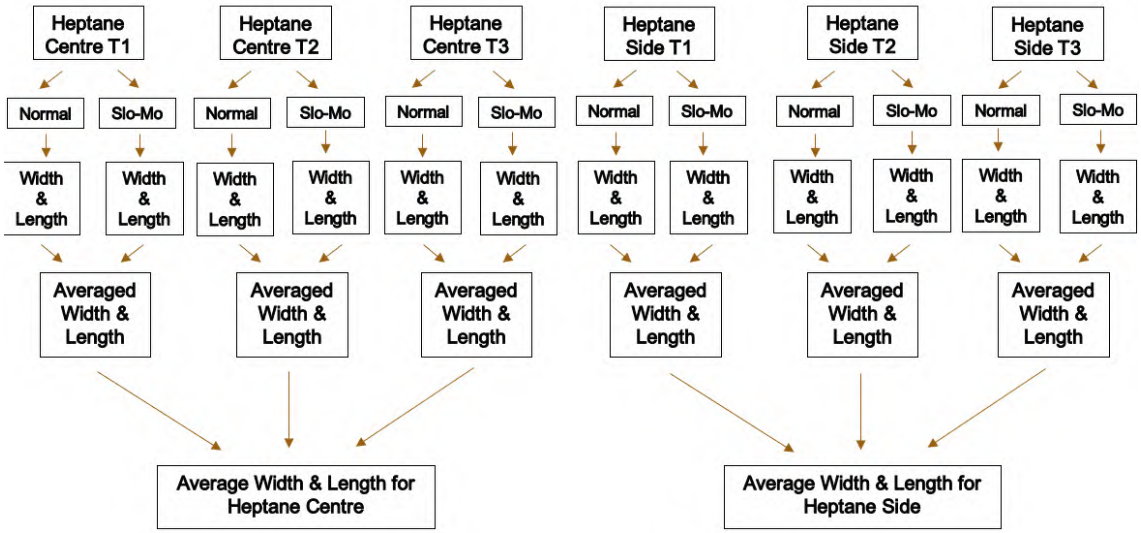

Figure 5.27: Averaging procedure of flame length's video analysis results.

5.3 Non Ceiling Bounded Flame Height Calculations

In order to compare the results obtained in this work to results from literature presented in the following chapters, the non ceiling bounded flame height needed to be determined. In particular, the correlation by Heskestad [30] presented in Chapter 3 was utilized and is shown in Equation 5.2.

$$\frac{H_f}{D} = 0.235\dot{Q}^{2/5} - 1.02 \tag{5.2}$$

This correlation was utilized in this work for both fuels and burners in the centre position of the two different ceiling setups. The correlation was not applied when the fire was placed in the side position: as mentioned previously, in these cases the effect of the side wall needed to be considered. Flame length calculations for the cases with the sidewall bounding were performed using Equation 5.3 [38].

$$H_f = (1.681 - 0.005P)\left(0.235(\beta\dot{Q})^{2/5} - 1.02D\right) \tag{5.3}$$

where H_f is the total flame height of the wall bounded fire, β is the mirror coefficient that is a correction factor that accounts for the wall or corner bounding (β = 1.6 for wall fires, β = 2.4 for corner fires), P is the operating pressure value in kPa, Q is the heat release rate in kW and D the fire source diameter in meters.

As discussed in Chapter 3, Heskestad's model is not intended for momentum driven flows but still provides reasonable results. For this reason, the correlation put forwards by Heskestad and its adaptation for the wall bounded case have been used to determine H_f for both heptane and propane tests. While for the propane tests the results may not be entirely accurate, they are deemed acceptable. Furthermore, while equations that describe flame lengths of momentum driven flows can be found in literature for free burning fires, correlations that account for the wall bounding effects have not been identified. It is therefore expected that the results presented in the following chapters are subject to some limitations. Further research and testing using the momentum driven flow equations for the propane case may yield more accurate results and a better representation of the momentum driven flow phenomena.

Chapter 6

Comparison of Results

6.1 Flame Extensions

In previous chapters the results obtained from the experimental campaign for both the flat ceiling and curved ceiling setups were discussed. Now a comparison between the flame extensions measured under the two ceiling geometries is performed. In Table 6.1 a summary of all flame lengths found from the tests it displayed.

Fuel	**Ceiling Type and Position**	**Flame Extension Under Ceiling (L_f) [m]**	**HRR [kW]**
Heptane	Flat, Centre	0.328	59.9
Heptane	Flat, Elevated Centre	0.405	80.4
Heptane	Flat, Side	0.283	48.7
Heptane	Flat, Elevated Side	0.354	69.6
Heptane	Tunnel, Centre	0.341	61.6
Heptane	Tunnel, Side	0.304	49.2
Propane	Flat, Centre	0.354, 0.397, 0.486, 0.545	40.1, 50.8, 62.1, 94.2
Propane	Flat, Side	0.384, 0.420, 0.511, 0.577	42.3, 53.4, 65.2, 96.2
Propane	Tunnel, Centre	0.359, 0.390, 0.493, 0.518	40.7, 52.4, 63.9, 100.9
Propane	Tunnel, Side	0.483, 0.509, 0.559, 0.601	40.8, 51.3, 63.8, 100.5

Table 6.1: Summary of flame lengths from the performed tests under the flat and cuved ceiling geometries.

The flame length data shows that in the flat ceiling tests, the elevated heptane pool fire produces the longest flame extensions. Due to the increased radiative feed-

back produced by the setup's geometry and the elevated position, the increased mass loss rate of the fuel results in higher HRRs and larger flames. From the curved ceiling tests, the longest flame length is found from experiments performed using the propane burner. This is due to its momentum driven flow and its significant contribution to the flow's extension beneath the curved ceiling.

The results from the experimental tests performed on the curved and flat ceiling setups have been plotted in Figures 6.1 and 6.2 respectively. The data has been presented in comparison with the normalized HRR, in a similar fashion to the data previously shown in Figure 3.1 in Chapter 3.

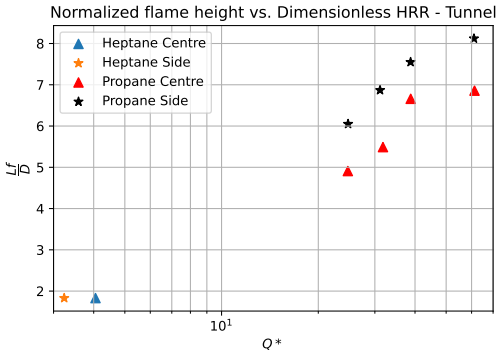

Figure 6.1: Normalized flame lengths resulting from the curved ceiling tests.

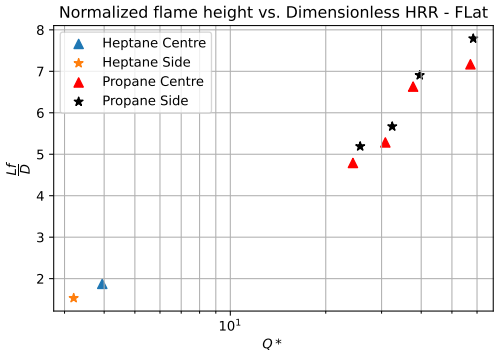

Figure 6.2: Normalized flame lengths resulting from the flat ceiling tests.

Analyzing the results, it is clear how in both cases the bouyancy driven flow of the hetpane tests yields significantly shorter flame extensions compared to the momentum driven flows of the propane tests. Focusing on the flat ceiling data in Figure 6.2, difference between the propane data for the central position and the side position is not significant. Looking at the ones found in Figure 6.1 instead, the difference between the flame length in the side and centre position is clear. As explained previously, the flame extension here is significantly increased by the combined effect of the momentum component of the gas burner and the ceiling's

curved geometry. The evolution of the flame length presented in the graphs above can also be followed visually looking at Figures 5.2 to 5.23. Focusing on the axes of Figures 6.2, 6.1 and 3.1, the data from the performed tests would fall in the lower left part of the plot with literature experiments. This is as expected and it can be seen that the heptane pool fires falls in the *"Pool Fires"* range and the propane burner fires are placed higher towards the middle of the plot and closer to the *"Jet Flames"* shown in Figure 3.1.

Chapter 7

Flat Ceiling

7.1 Flame Length Models

In Chapter 2, relevant literature for the work presented in this project was identified. In particular, three models for the prediction of flame lengths under ceilings were identified: these models will be described and subsequently compared to the results from the experimental campaign performed as part of this Master thesis project.

7.1.1 You and Faeth, 1981

The first model taken under scrutiny in this work for the analysis of flame extensions under the flat ceiling was developed by You and Faeth [5]. In their study, they investigated the flame length development under the horizontal ceiling for both confined and unconfined setups thanks to the utilization of a removable curtain wall. An empirical correlation was developed based on the flame height in free burning condition and the effective ceiling height: You and Faeth's correlation can be seen in Equation 7.1

$$L_f/D = a\left[\left(H_f - H_{ef}\right)/D\right]^b \tag{7.1}$$

In the equation D, L_f, H_f and H_{ef} are the equivalent diameter of the fire source, the flame length under the ceiling, the flame height in free combustion and the ceiling effective height respectively. The coefficients a and b differ for the two ceiling confinement cases and are a = 0.50 and b = 0.96 for an unconfined ceiling and a = 0.69 and b = 0.89 for a confined ceiling. In both cases, a free burning plume is tested: in the unconfined case, no curtain wall was placed around the ceiling while in the confined case the wall curtain was positioned. Their results concluded that the flame extensions beneath the flat ceiling were 20–40 % longer for the confined case. This is because the reduced oxygen concentration resulting from the placement of the curtain required the un-burnt fuel to extend further to fully combust, resulting in the larger flame length.

7.1.2 Gao et Al. 2017

The work done by Gao et Al. [37] was carried out in a 1/6th scale model tunnel with the fire source positioned against the walls at different heights above the ground. Based on the work from You and Faeth, they examined the temperature distribution and transverse ceiling flame length of a sidewall confined tunnel fire under a flat ceiling. Equation 7.2 below correlates the results found by Gao to the work of You and Faeth.

$$L_{\mathrm{f}}/D = 1.21\left[\left(H_{\mathrm{f}} - H_{ef}\right)/D\right]^{0.57} \tag{7.2}$$

This adaptation of the work by You and Faeth though did not account for the transverse impinging of the flame and the correlated physical processes. Gao in fact

determined that the flame impingement is directly related to the distance of the burner from the ground and the heat release rate: in particular, higher values of HRR and smaller distances of the burner from the ground, the longer the flame extension under the ceiling. It was determined that the flame length under the ceiling depended on the unburned part of the fuel at the impinging point; in particular, the more the unburned fuel, the longer the ceiling flame length [37]. This led to the development of a new correlation that accounted for the unburnt fuel propagating beneath the ceiling.

The heat release rate produced by the unburnt fuel under the ceiling, Q_{ef}, was therefore calculated by obtaining the relation between the flame volume and heat release rate, shown in Equation 7.3 with Q being the total heat release rate of the fire in kW, H_f the flame height without ceiling and H_{ef} the free height of the setup.

$$\frac{Q_{\mathrm{ef}}}{Q} = \frac{\left(H_{\mathrm{f}} - H_{ef}\right)^3}{{H_{\mathrm{f}}}^3} \tag{7.3}$$

The flame extension length under the ceiling can then be predicted by Equation 7.4 below

$$\frac{L_f}{D} = 2.3 Q_{ef}^{*1/4} \tag{7.4}$$

where L_f and D represents maximum flame length under ceiling and equivalent diameter of fire and Q_{ef}^{*} is the dimensionless HRR calculated using Equation 7.5.

$$Q_{\mathrm{ef}}^{*} = \frac{Q_{\mathrm{ef}}}{\rho_\infty \mathrm{c}_p T_\infty \sqrt{g} D^{5/2}} \tag{7.5}$$

7.1.3 Zhang et Al. 2019

The third model used to assess the flame length under the flat ceiling was proposed by Zhang et Al. [16]. In their work, a series of experiments were carried out in order to assess the flame extensions under an inclined ceiling for wall-attached fires. Different heat release rates, fire to ceiling heights and ceiling inclination angles (-20°to 20°) were tested. Illustration of the tests they performed using different inclination angles of the ceiling are represented in Figure 7.1. Results from the tests showed differences with similar work on non wall bounded fires and a strong variation resulting from the ceiling inclination angle.

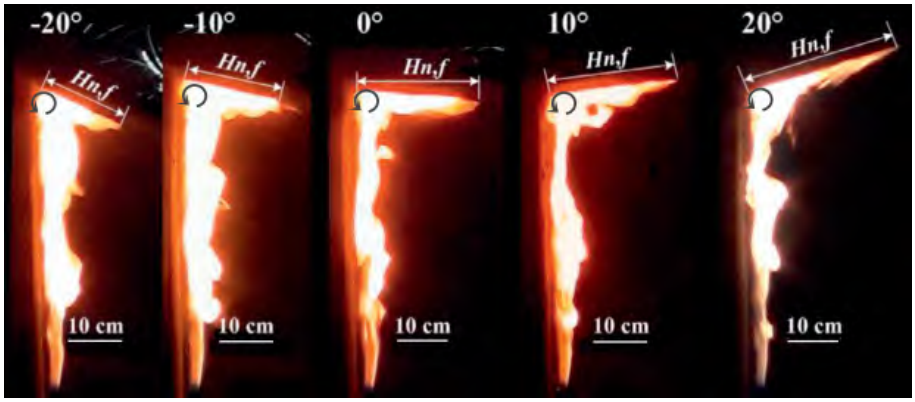

Figure 7.1: Tests performed by Zhang et Al. using the inclined ceiling at various inclination angles [16].

Their work yielded a new correlation that expresses the flame lengths in terms of the non ceiling bounded flame height H_f, the ceiling height H_{ef} and the inclination angle of the ceiling θ. The expression is shown in Equation 7.6:

$$\frac{L_f}{H_{ef}} = 0.91 \left(\frac{1 + \sin(\theta)}{2} \frac{H_f - H_{ef}}{H_{ef}} \right) \tag{7.6}$$

7.2 Results

7.2.1 Flame Length

The flame length values obtained from the video analysis process and used to obtain results that could be compared to the previously mentioned correlations, are summarized in Table 7.1 below.

Fuel	**Ceiling Type and Position**	**Flame Extension Under Ceiling (L_f) [m]**	**HRR [kW]**
Heptane	Flat, Centre	0.328	59.9
Heptane	Flat, Elevated Centre	0.405	80.4
Heptane	Flat, Side	0.283	48.7
Heptane	Flat, Elevated Side	0.354	69.6
Propane	Flat, Centre	0.354, 0.397, 0.486, 0.545	40.1, 50.8, 62.1, 94.2
Propane	Flat, Side	0.384, 0.420, 0.511, 0.577	42.3, 53.4, 65.2, 96.2

Table 7.1: Summary of flame lengths from the performed tests with the flat ceiling.

These lengths correspond to the L_f parameter in the correlations. From the Table, one can see how the flame lengths obtained in the heptane tests for the central position are larger than those for the side one. When positioned flush to the wall, the reduced entrainment affects both the flame development and the heat release rate [30]. This positioning also affects the combustion efficiency which is lower, resulting in the lower HRR values that were measured. The elevated heptane tests produce longer flames than the non-elevated case. This can be attributed to the fact that due to the reduced distance between burner and ceiling, the unburnt fuel needs to travel a longer distance after impinging on the ceiling before combusting completely. Furthermore, since the elevated position is closer to the ceiling, heat feedback enhances combustion producing a higher heat release rate and consequently longer flame. Similarly to the non elevated cases, also here due to the reduced entrainment in the side position, the flame length is shorter than in the central one. Another difference can be found by comparing the heptane flame lengths and the ones from the propane tests. In the latter cases, the flame is much longer: this is due

to the flow characteristics that differ for the two types of fuels. Recalling previous discussions, the propane burner is characterized by a momentum driven flow while the heptane one has a buoyancy driven flow. This difference results in larger flame lengths for the propane burner when comparing similar heat release rate values. It can be noted that another effect of the propane's momentum driven flow is that the flame resulting from the side positioning is longer than the one from the centre. The longer side flames are the result of unburnt fuel that needs to travel under the ceiling to fully combust [19].

You and Faeth 1981

The comparison between the results from the tests with the work by You and Faeth [5] and the adaptation of their work proposed by Gao et Al. [37], are shown in Figures 7.2 and 7.3 below.

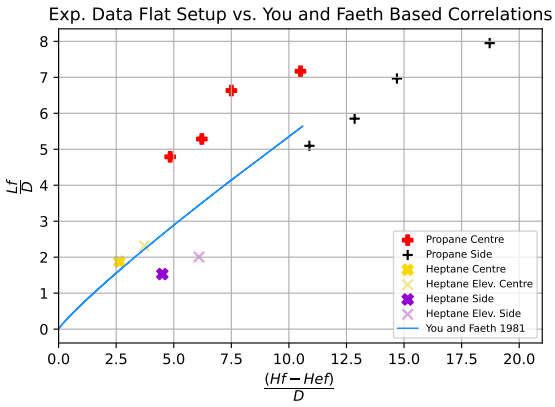

Figure 7.2: Comparison between test results for the flat ceiling setup with the You and Faeth model.

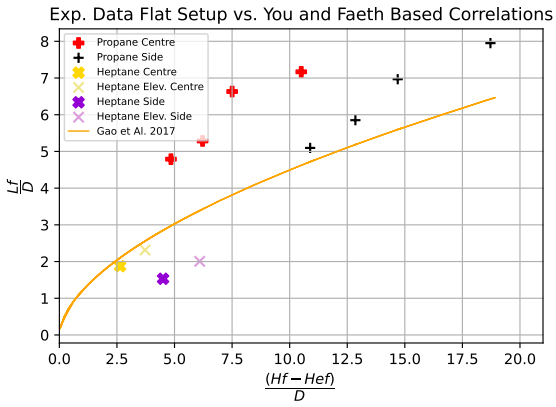

Figure 7.3: Comparison between test results for the flat ceiling setup with the adaptation presented by Gao of You and Faeth's model.

It is important to keep in mind that in the work by You and Faeth an unbounded free burning fire was used, while in the work by Gao et Al. a wall bounded fire was tested instead. One would therefore expect the results from the centre location test to follow the You and Faeth correlation while the side location ones to be similar

to Gao's adaptation. The heptane centre tests follow You and Faeth's linear correlation closely while the propane centre ones do not: it is interesting to see how in Figure 7.2 the centre values for propane still follow the same linear trend but are shifted towards higher values. This can be understood by considering the quantity plotted on the y axis, which is the ratio of the flame extension under the ceiling by the burner's equivalent diameter. Since the propane burner's equivalent diameter is considerably smaller than the heptane's, the data gets shifted upwards. Additionally, recalling the results from Table 7.1, we can see that the flame length under the ceiling for propane is larger than that found for heptane which further explains the difference in the results. Referring to the discussion on the HRRPUA quantity from Chapter 5 and considering that the experiments conducted by You and Faeth were not performed using gas burners, these differences can be expected.

With regards to the data for the side position, it can be seen in Figure 7.3 that the heptane data does not follow the results found by Gao et Al.: for propane instead, Gao's correlation is resembled with some error margin. The similarities can be attributed to the fact that the wall bounding is common to both the experiments and Gao's work; what is more, in their work Gao et Al. also use gas burners to perform the tests. The discrepancy between the correlation and the results on the other hand can be attributed to differences in the experimental setups, especially regarding the burner's characteristics. Gao et Al. use a burner with a characteristic diameter of 0.15m [37] which is twice the size of the one used in this work: this difference can therefore be the cause of the discrepancies seen in the data.

Gao et Al. 2017

After finding an adaptation of You and Faeth's work, Gao et Al. determined that the transverse impinging flame was not accounted for in the correlation. As explained

previously, they therefore put forward a new correlation that takes into account the unburnt fuel propagating beneath the ceiling which affects the flame extension. In Figure 7.4 the comparison between the test data and the new flame extension relationship developed by Gao et Al. are shown. There is a difference between the correlation proposed by Gao et Al. and the experimental data. In particular, the data is mostly shifted towards higher L_f/D values. For the heptane tests, the data is the closest to Gao's curve: the similarity is due to the similar burner diameter sizes of the heptane tests and the tests performed in the literature which measure 0.18m and 0.15m respectively. The slight difference instead is attributed to the difference in flame lenght: the momentum driven flow of a propane fire such as the one used by Gao in their experiments will produce a a larger flame height compared to the buoyancy driven flow resulting from the heptane fire.

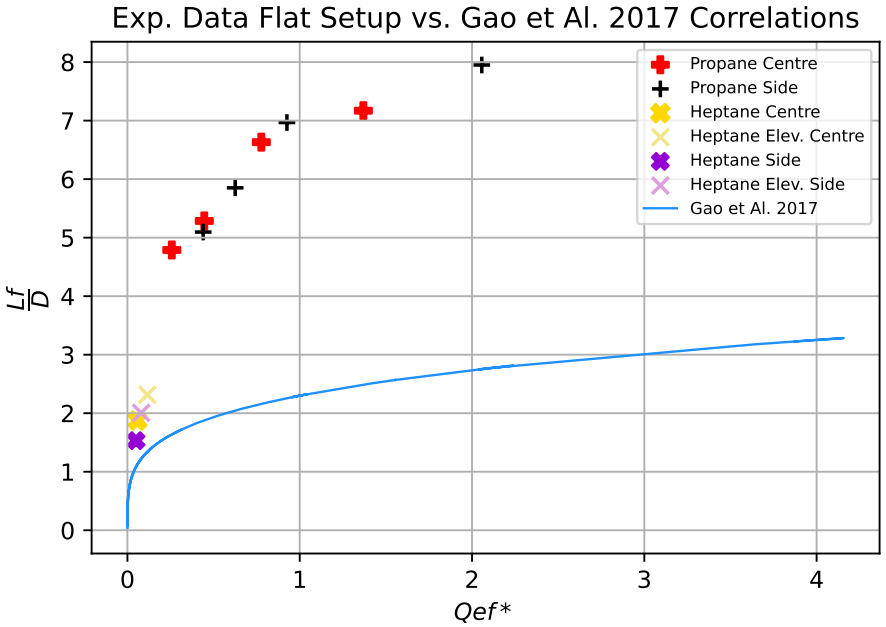

Figure 7.4: Comparison between test results for the flat ceiling setup with the Gao et Al. model.

The propane test data is shifted significantly higher instead. As mentioned in

the discussion of the results from the You and Faeth comparison, the diameter of the propane burner used in the experimental tests of this work is half that of the tests by Gao et Al. and causes the differences seen in Figure 7.4. One can also see how the flame extension for the side positioning of the fire are longer than the ones for the centre position: the black crosses are positioned higher than the red ones for the same test.

Zhang et Al. 2019

Finally, the data was compared to the results found by Zhang et Al. [16]. Recalling the correlation they came up with in their work, shown previously in Equation 7.6, for the flat ceiling setup θ was set to 0°.

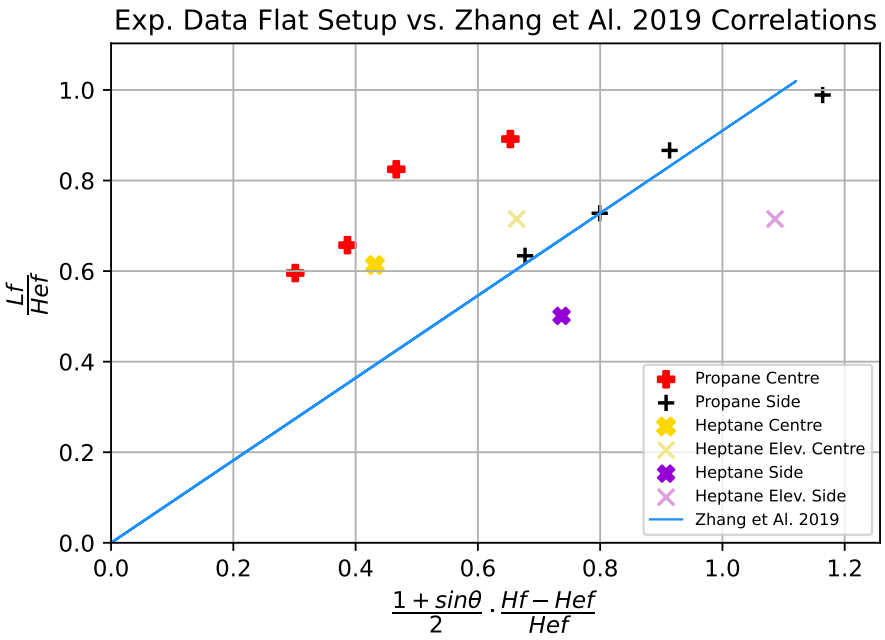

Figure 7.5: Comparison between test results for the flat ceiling setup with the Zhang et Al. model.

Like in the experiments carried out by Gao et Al., Zhang et Al. used a wall bounded fire; therefore it is expected that the experimental data found in this work

for the burners positioned flush to the sidewalls will follow Zhang's correlation more closely than the data for the central position. Figure 7.5 shows the relation between the data and the third correlation taken into consideration. As expected, the results obtained from the fires positioned on the side of the setup show consistency with Zhang's equation: this is more evident for the gas burner, while the heptane for the side position is slightly shifted downwards. This shift downwards is attributed to the shorter flame lengths obtained in the heptane tests: looking at the quantity plotted on the y axis, $\frac{L_f}{H_{ef}}$, since the effective height of the compartment is the same for each test in the flat ceiling setup, smaller flame lengths will yield smaller $\frac{L_f}{H_{ef}}$ values as in the heptane case. The determination of the flame's extension under the ceiling through video analysis also affects the results since only the side view of the experiment is obtained and analyzed. If a front view were considered for the side wall positioned fires, one would see how the flames extend sideways [37] creating an inverted cone with the burner being its top. This occurs since the reduced entrainment caused by the sidewall makes the fire spread to combust: this phenomena is not captured nor quantified in this work, therefore presenting a limitation to the obtained results.

A similar reasoning can be applied for the data from the centre setup, where the data is shifted to the left indicating that the variation is caused by the term on the x axis. Since $\theta = 0°$, the sine term disappears the data is dependant on the ratio between the difference of flame height obtained from non-ceiling bounded combustion with effective height of the setup and the effective height of the setup. Therefore, for the centre position tests, the non-ceiling bound flame length is shorter than that of the side positioned tests. Additionally, for both fuel types and positions some deviations can be attributed also to how the non-ceiling bound flame has been calculated. As discussed in previous sections, this quantity was calculated empirically utilizing the

correlations presented in Equations 5.2 and 5.3 which present some limitations for the tests performed in this work.

7.2.2 Temperatures

Temperatures were measured during the tests performed in the flat ceiling setup using 11 K-type thermocouples placed under the ceiling. Since the thermocouples had been previously utilized for other tests in the lab, a degree of error is expected in the resulting temperature measurements. The placement of the thermocouples has been shown in previous chapters in Figures 4.3. In Figures 7.6 and 7.7 the results of the temperature measurements are shown. In the Figure on the left, the thermocouples are placed across the setup's cross section while the Figure on the right represents the temperatures measured along the length of the setup. For these tests the burner was placed in the central position. In both Figures, the central thermocouple measures the highest temperature since the fire impinges on the ceiling at that point; moving away from the centreline the temperature decreases. In Figure 7.7 the same trend can be seen. Looking at Figure 7.6, one can notice that for the propane tests the highest flow rate yields the highest temperatures. With regards to the heptane tests, when the burner is elevated, higher temperatures are reached than in the non elevated case due to the closer positioning to the thermocouples. The blue stars represent the average flame length measured in the tests. As was found in the flame length results, the largest flame lengths are produced by the propane burner with the largest and second largest flows.

One can notice how for the heptane tests the temperature at which the flame length is measured is similar around 700°C; similarly for gas flow 1,2 and 3 the flame length temperature falls between 400°C and 450°C; for the highest gas flow, the temperature at the flame length is approximately 750°C. Recalling the descrip-

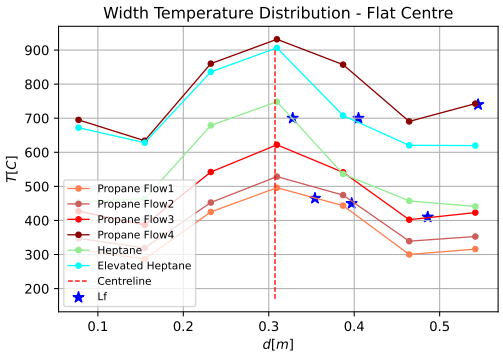

Figure 7.6: Central burner position temperature distribution along setup's width.

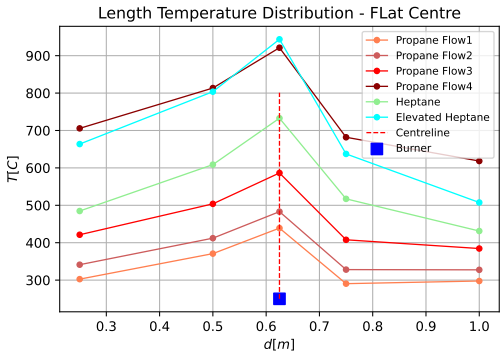

Figure 7.7: Central burner position temperature distribution along setup's length.

tion of the setup from Chapter 4, we can understand why in Figure 7.6 the points at the left of centreline are higher than the ones on the right. The right side of the setup had a partially closed side as shown in Figure 4.4; the left side instead was completely open and can be seen in the pictures taken of the tests in Figures 5.8 through 5.15. Since the left side of the tunnel was completely open, after impinging the ceiling the flow used this outlet as the one with least resistance. This results in higher temperature readings on the left side of the flat ceiling setup. When looking at the smallest flow rate, the temperatures at each end appear to be similar meaning that in this case the partially closed opening is also used for the flow to escape from.

The results from the temperature measurements when the burner is placed in the side position flush to the sidewall of the setup are presented in Figures 7.8 and 7.9. Also in this case the thermocouples placed above the fire measure a temperature close to 900°C which then decreases moving away from the impingement point as the flame extends. The highest gas flow of the propane burner once again yields both the highest temperature values and the longest flame extension: the temperature at this point reaches 500°C. The lower gas flow rates reach 300°C at the flame length

point. In the heptane tests instead the elevated case yields higher temperature values due to proximity of the flame to the thermocouples. Also in this case one can see how the flame length resulting from the propane tests is longer than the one found from the heptane tests.

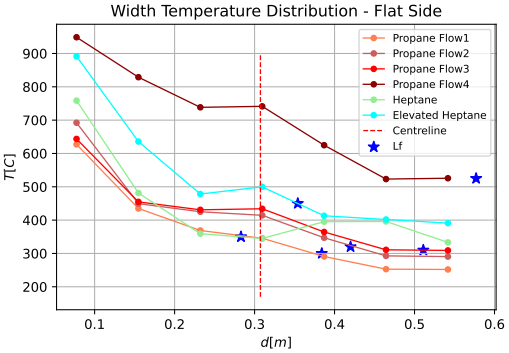

Figure 7.8: Side burner position temperature distribution along setup's width.

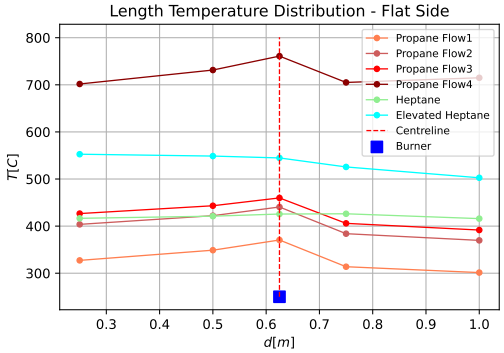

Figure 7.9: Side burner position temperature distribution along setup's length.

Looking at Figure 7.9 similar results to those found in Figure 8.8 can be observed. The temperatures in this case are lower than for the tests where the burner was placed in the middle of the setup: since the thermocouples are placed lengthwise along the longitudinal centreline (Figure 4.3, the fire is no longer directly over the thermocouples. The effect of the partially closed side is also seen in these tests results.

Chapter 8

Curved Ceiling

8.1 Flame Length Models

Similarly to the structure in Chapter 7, in this chapter the models found in literature and the results obtained in the experimental tests for the curved ceiling setup are discussed. The curved ceiling setup is also referred to as the tunnel setup in the following.

8.1.1 Zhang et Al. 2019

This model has already been outlined in Chapter 7 and will not presented again in this Chapter. Since Zhang's work was performed on an inclined ceiling and a correlation dependent on ceiling inclination angle was obtained, it was adapted for the curved ceiling in this work. For the curved ceiling setup, the inclination angle θ was taken as the angle of the tangent line at the impingement point. Figures 8.1 and 8.2 show a schematic of the setup and the impingement angle for the two burner positions used in the tests. With simple trigonometry, the angle for the side setup is found to be $90 - \theta = 90 - 33.7 = 56.5°$while for the central setup it is of

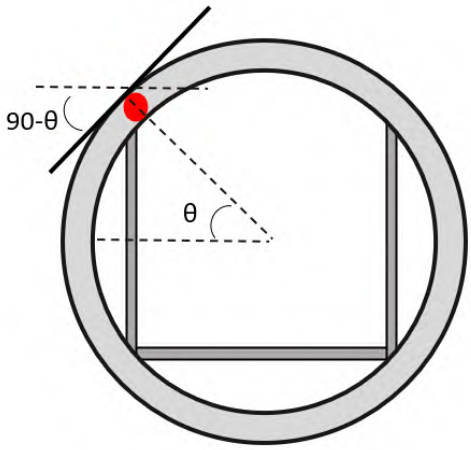

Figure 8.1: Schematic of side tunnel setup impinging angle.

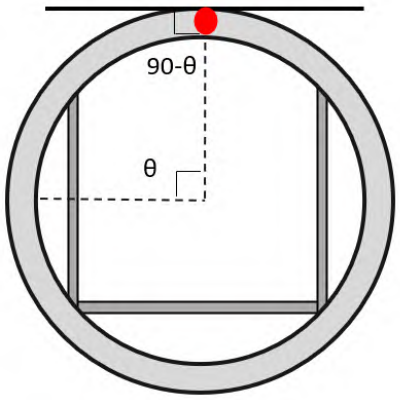

Figure 8.2: Schematic of side tunnel setup impinging angle.

Figure 8.3

$90 - \theta = 90 - 90 = 0°$. The same correlations discussed in Chapter 7 were then followed utilizing the newly mentioned angle values.

8.1.2 Pan et Al. 2020

The second model considered in the study of the curved ceiling setup is the result of the work from Pan et Al. 2020, A series of experiments was carried out to study the effect a curved sidewall had on the flame shape using a 1/4 scale concrete model. Burners with characteristic diameters from 0.15m to 0.3m and using oil as a fuel were tested; their positioning inside the setup was also varied with different distances from the centre line, but the position flush to the wall was not studied. Taking into account the expression put forward by You and Faeth [5] for the flat ceiling case, Pan et Al. adapted the correlation to the curved ceiling setup. The new expression is shown in Equation 8.1

$$L_f/D = 1.47\left[\left(H_{\mathrm{f}} - H_{ef}\right)/D\right]^{0.22} \tag{8.1}$$

As shown in the Equation above, the relation shows the dependence between flame length L_f, the fuel source's characteristic diameter D, the flame's height in non-ceiling bounded conditions H_f and the free height between the burner and the flame impingement point on the ceiling H_{ef}. The coefficients that characterize the dependence between the different parameters for the tunnel setup differ from the flat cases proposed in [5] and [37] and are larger for the curved ceiling case. Pan et Al. also determined that the transverse flame length under the ceiling is the result of the unburnt fuel extending after impingement [19]. Furthermore, it was determined that the length of the flame extension depends on the fire's heat release rate: in particular, higher HRR values produced longer extensions. The the empirical model does not take into account the effect of the curved ceiling on the flow's buoyancy component though, implying that not all effects contributing to the flame extensions are expected to be considered by this correlation.

8.1.3 Pan et Al. 2022

The third model used to analyze the results found from the flame video analysis of the curved ceiling experiments comes from work performed by Pan et Al. 2022. The experimental setup used in their study consisted of two curved ceiling tunnels with different cross sections: one 20m long, 0.9m outer radius, 0.75m inner radius and the other 100m long, 1.1m inner radius both made out of concrete. Tests were performed at different heights from the curved ceiling and distances from the centreline of the setup; the fuels used were heptane, ethanol, methanol and cable stacking as solid fuel.

In their new model, they take into account the buoyancy effect of the fire plume under the curved ceiling: this parameter was not considered in previous studies but

has a significant impact when considering a curved ceiling setup [24]. A theoretical and experimental investigation was then performed to determine the flame length: in particular, the analysis of the effect of unburnt fuel and of the varying buoyancy flow component were studied. To do this, a momentum balance equation was utilized. Effective HRR was expressed accounting for entrained air mass and unburnt fuel flows and assuming a linear relation between ceiling jet velocity and entrained air. The new equation describing the flame lengths beneath the curved ceiling is shown in Equation 8.2.

$$\begin{cases} (f_c)^{1/2}\,\frac{L_f}{D} = 8.59\left[\frac{(1+\cos\theta)}{2}V_{fu}/V_f \cdot \frac{(Q/D^2)}{\rho_\infty(\Delta H_c/s)\sqrt{gH_{ef}}}\right] 1/2 \\ f_c = \sqrt{1+\left(\frac{R}{3H_{ef}}\right)\left\{(\sin\theta)^3 - 3\sin\theta - \left[\sin\left(\theta+\frac{L_f}{R}\right)\right]^3 + 3\sin\left(\theta+\frac{L_f}{R}\right)\right\}} \end{cases} \tag{8.2}$$

In the Equation, L_f is the flame length, D the burner's characteristic diameter; θ the angle between the setup's centre and the flame impingement point as shown in Figures 8.1 and 8.2; the ratio V_{fu}/V_f is the ratio of cut-off flame volume by the curved ceiling and free flame volume without ceiling (used to calculate the unburnt fuel mass flow based on the fuel mass flow from fire source); Q is the fire's heat release rate, ρ_∞ the density of air; $(\Delta H_c/s)$ is the heat release per mass consumed air (kJ/kg), g is the gravitational constant; H_{ef} the clearance height between the flame's impingement point and the fuel source; R the radius of the curved ceiling setup.

From their study, Pan et Al. determined that a shorter clearance height between the fire and the tunnel's ceiling produces longer flame lengths. As found in previous work [19], the reason for this longer extension is the unburnt fuel moving under the

ceiling after impingement. Moreover, the effect of the fire's buoyancy component along the ceiling affects also the flame's length. Therefore, thanks to their work, significant influence of the curved ceiling geometry was found on the flame length, the unburnt fuel and the fire's buoyancy component.

8.2 Results

8.2.1 Flame Length

In Table 8.1 the flame lengths obtained from the video analysis of the curved ceiling tests are listed. The results found in this setup are similar to the ones found in Chapter 7. The flame lengths produced by the buoyancy driven heptane fire are shorter in the side position due to the reduced entrainment.

Fuel	**Ceiling Type and Position**	**Flame Extension Under Ceiling (L_f) [m]**	**HRR [kW]**
Heptane	Tunnel, Centre	0.341	61.6
Heptane	Tunnel, Side	0.304	49.2
Propane	Tunnel, Centre	0.359, 0.390, 0.493, 0.518	40.7, 52.4, 63.9, 100.9
Propane	Tunnel, Side	0.483, 0.509, 0.559, 0.601	40.8, 51.3, 63.8, 100.5

Table 8.1: Summary of flame lengths from the performed tests with the curved ceiling.

The propane burner instead produces longer flames in the side position due to the combined effect of the unburnt fuel travelling under the curved ceiling and the fire's momentum component. The momentum component of the flow impacts the results significantly more for the same HRR in this case and can be seen in the Table above.

Zhang et Al. 2019

When comparing the experimental results to the relationship proposed by Zhang et Al. not all the data follows the proposed linear trend. Results for the heptane tests

positioned flush to the side of the tunnel and results from the work by Pan et Al. (magenta data points taken from Figure 10 in their work) [24] follow the relationship closer than the central burner position test data.

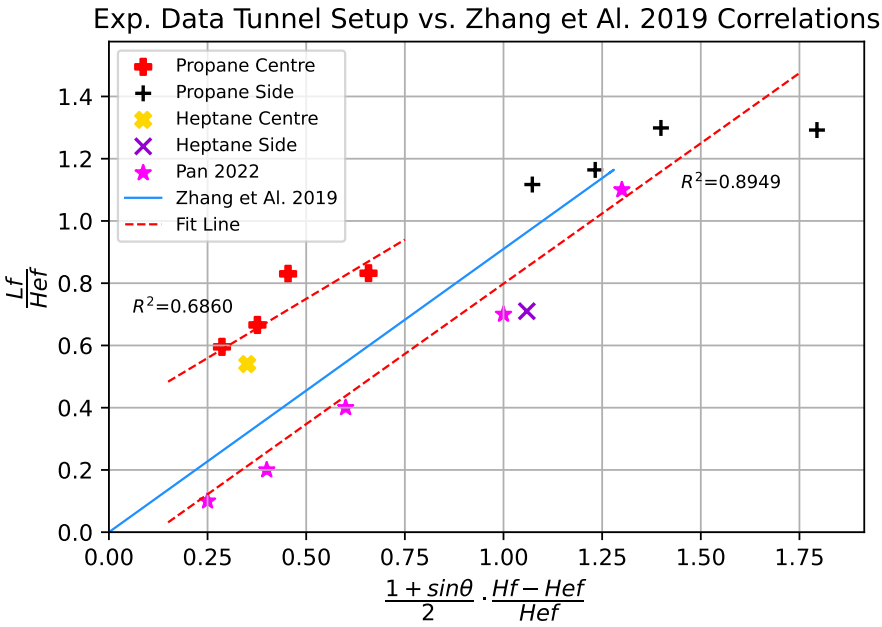

Figure 8.4: Comparison between test results for the curved ceiling setup with the Zhang et Al. model.

The close relationship between these two data-sets can attributed to the same fire location used in each test. As mentioned previously, Zhang's model takes into consideration the fire's buoyancy component but assumes it is constant; thanks to the work by Pan et Al. [24], it was found that the buoyancy component is not stable under the curved ceiling. The similarities between the tests using heptane as a fuel and Zhang's relation could therefore also be attributed to the fact that the buoyancy component of the heptane fires does not vary significantly along the ceiling. The differences seen in Figure 8.4 when looking at the momentum driven flow of the propane tests instead can be associated to the strong momentum variation due to the nature of the flow and the ceiling's geometry. Furthermore, recalling

the equation put forward by Zhang, Equation 7.6, the dependence from the ceiling inclination angle is clear. Here, the validity of their equation falls in the range of angles between -20°and 20°. When the burner is placed in the central position, the inclination angle is set to 0°, which falls within the reange of validity of Zhang's correlation. On the other hand, differences can be expected for the side position since the inclination angle is 56.5°. As shown in Figure 8.4, the experimental data from the side position and the test data from the Pan 2022 tests can be better represented using the dashed fit line on the right. The line represents a linear adaptation of Zhang's original correlation and is shown in Equation 8.3.

$$\frac{L_f}{H_{ef}} = 0.902 \left(\frac{1 + \sin(\theta)}{2} \frac{H_f - H_{ef}}{H_{ef}} \right) + 0.104 \tag{8.3}$$

The fit has $R^2 = 0.8949$ indicating a good fit between the data from the side position tests and the fit line. The results from the centrally positioned burner tests instead can be represented more accurately using Equation 8.4 which provides an $R^2 = 0.6860$ value.

$$\frac{L_f}{H_{ef}} = 0.761 \left(\frac{1 + \sin(\theta)}{2} \frac{H_f - H_{ef}}{H_{ef}} \right) + 0.369 \tag{8.4}$$

Considering the newly found fitting correlations, it is deemed that Zhang's correlation needs to be modified to Equations 8.3 and 8.4. In this way, the effects that result from the change in position of the burner and the momentum driven flows can be considered comprehensively. Overall though, while Zhang's model considers most factors affecting flame extensions, the non-consideration of the changing buoyancy component results in an incomplete representation of all phenomena that impact the results.

Pan et Al. 2020

The correlation proposed by Pan et Al. 2020 [19] was then compared to the test data. Figure 8.5 shows the test data resulting from the experiments carried out in this thesis project, results obtained by Pan et Al. 2022 (Figure 9 in their work) [24] and the correlation put forward by Pan et Al. 2020 represented by Equation 8.1. The first interesting result that can be seen looking at the data is that the flame length produced by the heptane tests are much lower compared to the propane test ones. This can also be seen in Table 8.1 and referring to previous discussions is attributed to the difference in flow characteristics, namely the momentum driven propane gas flow and the buoyancy driven heptane fire.

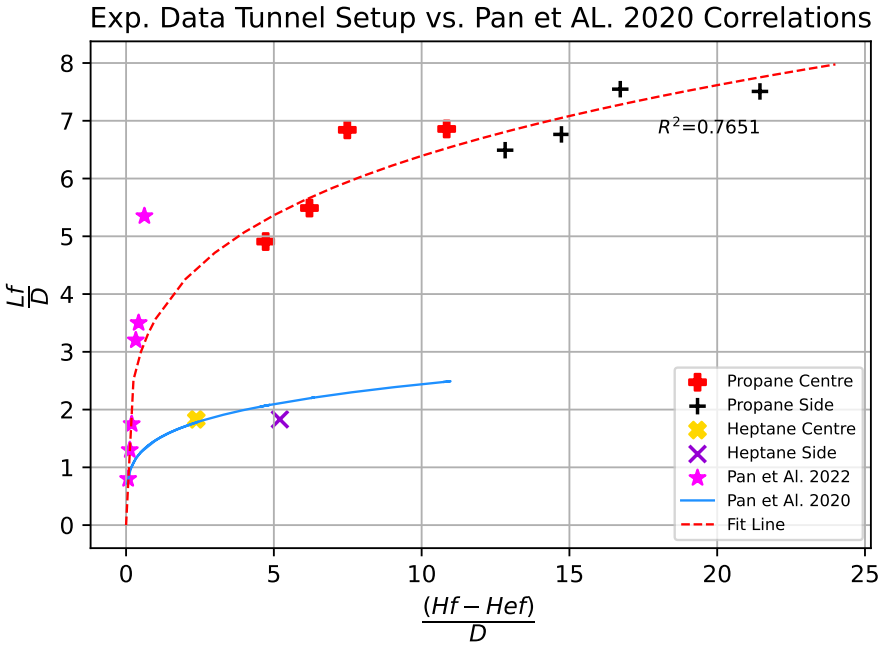

Figure 8.5: Comparison between test results for the curved ceiling setup with the Pan et Al. 2020 model.

The data also shows how despite using different fuels, the flames resulting from the side position extend more than for the centre position. After the flame impinges on the ceiling, the unburnt fuel travels under the ceiling until it is fully combusted.

The distance travelled in the central position is shorter since the flame is only limited by the ceiling itself; when the fire is positioned flush to the sidewall instead, the flame needs to travel further since it is limited both by the sidewall and the ceiling.

Looking at the results of the Pan et Al. 2022 tests which were also performed using heptane pool fires, we can see that their flame extensions are larger than the ones produced by the tunnel tests with the same fuel. This is because Pan et Al. 2022 tested smaller clearance height setups which result in longer flame extensions [24]. The model developed by Pan et Al. 2020 follows the heptane test data closely but does not represent the propane test results or the longer flame extensions found by Pan et Al. 2022. This discrepancy is attributed to the fact that also Equation 8.1 does not take into account the changing buoyancy component of the flow under the curved ceiling. While this model does not fully take into account all the effects that occur when a flame extends under a curved ceiling, by fitting the propane test data a new correlation is found and is shown in Equation 8.5. When comparing the newly found Equation 8.5 to that proposed by Pan et Al. shown in Equation 8.1, it can be seen how the multiplication coefficient in front of the equation is approximately 2.5 times larger: this difference accounts for the larger flame extensions obtained and for the momentum driven flow of the propane burner.

$$L_f/D = 3.57\left[\left(H_{\mathrm{f}} - H_{ef}\right)/D\right]^{0.25} \tag{8.5}$$

The exponent of the new correlation 0.25 does not differ significantly from the original 0.22, implying a close similarity between the two in terms of the correlation between flame length L_f and $(H_F - H_{ef})$. Additionally, the new correlation also closely represents the data found in the tests performed by Pan et Al. 2022. In their work, the comparison between their results and the correlation proposed by

Pan et Al. 2020 was discussed. In particular, it was found that their results did not follow the Pan et Al. 2020 model closely and this difference was attributed to the limited data that could be acquired from previous tests and different definition of flame length. Thanks to the new test data found performing the tests under the curved ceiling, a better general representation of the flame extension is found using Equation 8.5 with a corresponding accuracy that yields an $R^2 = 0.7651$ value.

Pan et Al. 2022

Finally, the experimental data was compared with the correlation developed from the work of Pan et Al. 2022 [24]. As described previously, the new model takes into account the important factor that is the changing buoyancy component of the fire along the curved ceiling: this parameter was not taken into account in previous correlations. The results are plotted in Figure 8.6 below.

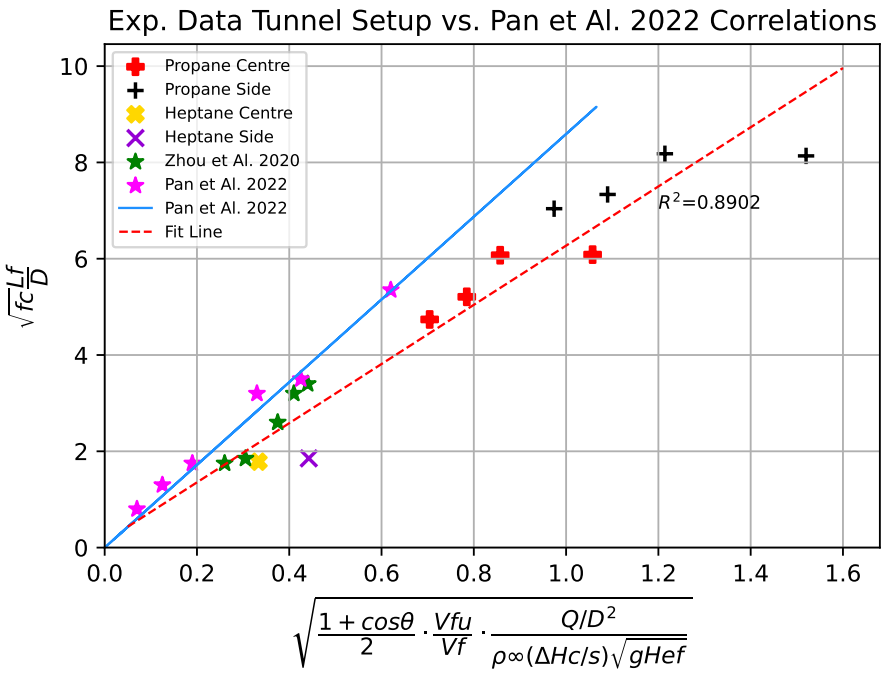

Figure 8.6: Comparison between test results for the curved ceiling setup with the Pan et Al. 2022 model.

In addition to the test data results and to the correlation developed by Pan et Al. 2022, also results from the tests of Zhou et Al. 2020 [39] have been included in the plot. In their work, Zhou et Al 2020 find the flame extension under the ceiling resulting from heptane pool fires. Similarly to previous results, also in this case the differences in flame extensions between the propane and heptane fuel types can be seen. Overall, the new correlation shows similarities with the test result data. A closer relationship is found with the heptane test data, since also in their work Pan et Al. 2022 utilize the same fuel source. The relation can therefore correlate buoyancy driven flows better than momentum driven ones, such as the propane burner. Equation 8.6 shown below represents the fit line seen in Figure 8.6 which fits both the propane test data results and the heptane test data results closer than the Pan et Al. 2022 model. This is shown by the $R^2 = 0.8902$ value that indicates a close relationship between the fit line and the test data.

$$\begin{cases} (f_c)^{1/2}\,\frac{L_f}{D} = 6.15\left[\frac{(1+\cos\theta)}{2}V_{fu}/V_f \cdot \frac{(Q/D^2)}{\rho_\infty(\Delta H_c/s)\sqrt{gH_{ef}}}\right]^{1/2} + 0.13 \\ f_c = \sqrt{1+\left(\frac{R}{3H_{ef}}\right)\left\{(\sin\theta)^3 - 3\sin\theta - \left[\sin\left(\theta+\frac{L_f}{R}\right)\right]^3 + 3\sin\left(\theta+\frac{L_f}{R}\right)\right\}} \end{cases} \tag{8.6}$$

Comparing the multiplication factor found for the new fit line of 6.15 with the original factor proposed by Pan et Al. 2022 of 8.59, it is clear that there is not much discrepancy between the two. This indicates that overall the correlation represents the flame extensions closely.

8.2.2 Temperatures

In the tests also the temperature under the ceiling was measured. These were performed to get a better understanding of how this quantity changes during the tests

and in relation to the flame extension. As mentioned in Chapter 4, 13 K-type thermocouples were installed in under the curved ceiling setup: nine were placed across the setup's cross section in correspondence with the burner and four along the setup's length. Figure 4.1 shows the thermocouple placement. The temperature distribution resulting from the fire in the centre of the setup are displayed in Figures 8.7 and 8.8. In Figure 8.7 the thermocouples are placed along the cross section of the setup while in Figure 8.8 the thermocouples are placed along its length. As should be expected, along the curved ceiling's cross section the temperature is higher at the centre where the fire impinges and decreases moving further away from the tunnel's centreline.

A similar fashion can be seen looking at the temperatures along the length of the setup. Since the thermocouples had already been used for previous experiments, some differences in temperature readings can be expected. This is clearer when looking at the second thermocouple from the left in Figure 8.8: this thermocouple clearly measures a higher temperature in all tests. An additional reason for the non-simmetrical results can also be attributed to how the test setup was placed in the lab. While the left side of the setup was facing an open area in the lab, the right side was facing a wall: this can be seen in the schematic of Figure 4.5 and could therefore have impacted the test results favouring the combustion gases to flow predominantly towards the unbounded side of the setup. In both figures we can see that the temperatures produced by the propane fires are higher than the heptane ones. Furthermore, the higher propane flow fire is associated with the larger temperature values. In Figure 8.7, the flame length is characterized by the blue stars. The flame length for the heptane tests is the lowest and as the propane flow increases so does the flame length. The temperatures at the flame point are constant at approximately 400°C except for the largest propane flow where the temperature

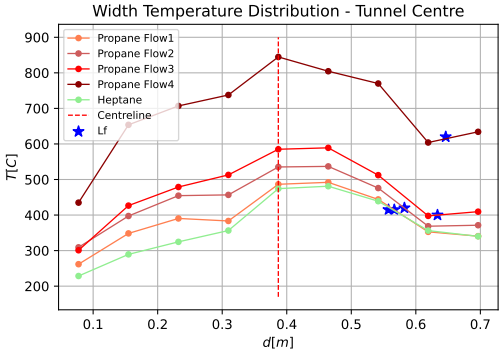

Figure 8.7: Central burner position temperature distribution along setup's width.

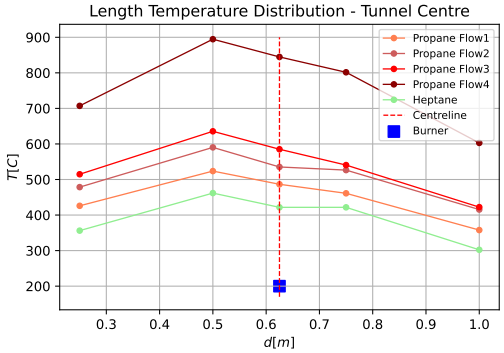

Figure 8.8: Central burner position temperature distribution along setup's length.

Figure 8.9

at the flame point is slightly above 600 °C. It is interesting to note that the flame length does not vary significantly for this last case, indicating that flows larger than Flow 3 (0.5 L/s) the flame length does not vary significantly. This can be further understood recalling Figure 5.22 where one can see how the flame begins extruding from the setup when gas flow 4 (0.75 L/s) is tested.

A similar analysis can be done for the temperature measurements taken when the fire is positioned flush to the wall in the side position. In this case, the thermocouples placed directly on top of the fire are the ones on the side in Figure 8.10 and similarly to the central position the maximum temperature registered at the impingement point is of approximately 900°C. From the impingement point, as the flame extends the temperatures decrease. The temperature reduction can be seen in Figure 8.10: here, similarly to the centre position case the highest temperatures are obtained from the propane tests using the highest gas flow rate. The heptane test temperatures are the lowest also for this burner position. Discrepancies in the thermocouple readings are once again attributed to defects of the devices that cannot be considered identical. The closenes of the righten side of the setup to a wall in the lab also affects

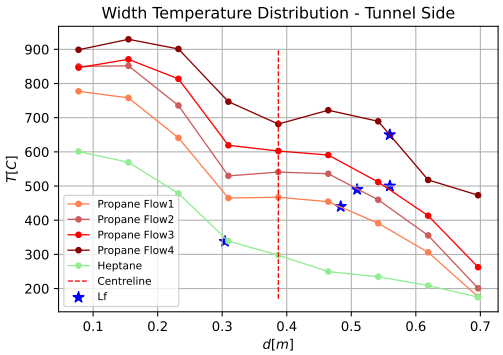

Figure 8.10: Side burner position temperature distribution along setup's width.

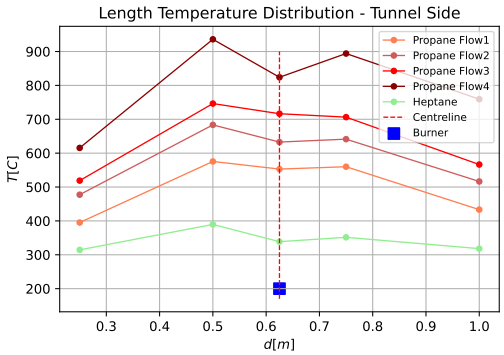

Figure 8.11: Side burner position temperature distribution along setup's length.

Figure 8.12

the ventilation inside the setup and consequently the temperature measurements. Also in this case, for the temperature readings measured along the setup's length and shown in Figure 8.11, the second thermocouple from the left shows a larger temperature value compared to the other thermocouples despite the fire not being directly above it.

Studying the flame's position compared to the centreline shown in Figure 8.10, it is clear also for this positioning of the burner that the heptane tests produce a smaller flame length compared to the propane tests. The temperature value at which the flame extension for the heptane case is also slightly lower than that found for the previous position: this difference can be attributed both to video analysis errors that produce the average flame length and to measurement differences of the thermocouples themselves. The propane temperature data at the flame length point is similar to that found for the central position. Also in this case for the largest flow rate case, while the flame length does not vary much the temperature at the flame point does. Once again, by visual inspection of Figure 5.23 we can see how at the largest flow rate the flames do not extend further beneath the ceiling but begin

projecting outside the setup. This explains why the temperature is higher but the flame length remains constant.

Chapter 9

Discussion

In this work, an in depth analysis on the phenomena of flame extensions under ceilings has been undertaken. The focus of the project was comparing the flame's extension length under flat and curved ceiling geometries. Two experimental scale models were utilized to perform the tests: a flat ceiling setup measuring 800x1200x680mm and a curved ceiling setup measuring 685x1200x680mm. The momentum and buoyancy driven flows of propane and heptane were used to determine the effect of the fuel source and flow characteristics on the flame extension. Central and flush to the wall positions were also tested. Data collected by the smoke extraction hood under which the tests were performed was used to calculate the heat release rate of the fires.

To measure the flame lengths resulting from the experimental campaign, videos of each test were taken. A Python video analysis code was developed in order to identify fire pixels in each video frame, determine the flame extension and draw conclusions about its behaviour beneath the ceilings. This step was crucial for the project since without it the in depth analysis could not have been performed. Despite this, the effect that the different setups had on the flame extensions could not be completely captured. Since the videos were only taken from the side of the setup,

only the flame extension compared to the setup's cross section was visible: how the flame developed across the setup's length was not considered, potentially resulting in the non-consideration of all flame characteristics. Furthermore, while the Python video analysis code captured the flame extension accurately based on the fire pixel colour ranges that were set, the effect that the variation of such parameter were not studied. In particular, a sensitivity analysis would bring greater insight on how the variation of the pixel colour range would affect the measured flame length.

Thanks to a comprehensive literature review, in depth insights were obtained regarding the different models used to represent flame behaviour when bounded by a flat or curved ceiling. It was determined that the flame extension phenomena under flat ceilings was extensively studied. Models by You and Faeth, Gao et Al. and Zhang et Al. were used to analyze the flame length results found experimentally and compare them to literature values. Less work was developed on the curved ceiling geometry. Correlations put forward by Zhang et Al. and Pan et Al. were adapted to the results found from the experimental campaign using linear regression. Several tests were performed using both flat and curved ceiling setups. A heptane pool fire and propane gas burner were used as fuels during the tests. in order to investigate which parameters affect the flame lengths, the position of the burners inside the flat and curved ceiling setups was varied between central and flush to the sidewalls; different gas flow rates were also tested to evaluate the effect of increased heat release rate on the flame extension. Since no free burn tests of the two fuel types were performed, empirical correlations from literature were used to determine the non-ceiling bounded flame heights. These are not intended for momentum driven flows such as the one produced by the propane burner: due to limited availability of mathematical models that can represent such flows, the former were used. Further interesting results could have been obtained by placing the burners in other interme-

diate positions or at different height levels from the ceiling. The utilization of larger burner dimensions and additional fuel sources could have also been interesting to test, giving further insights into their effect on the flame extensions.

Due to the reduced entrainment caused by the sidewall of the setup, the results for the flat ceiling indicated that the flame length was greater in the central position than in the side position. Additionally, because of the heat feedback produced by the setup's structure, increased heat release rate resulted in the elevated heptane tests producing longer flames than the non-elevated scenario. The fuels' flow properties also had an impact on the length of the flames; propane's momentum-driven flow led to longer flames, whereas heptane's buoyancy-driven flow led to shorter flames. The results matched the anticipated patterns found in correlations found in literature, with minor variances that may be attributed to different experimental settings and burner characteristics. With regards to the flame lengths obtained with the curved ceiling setup, the research demonstrated that the flame length is impacted by unburnt fuel and varying buoyancy component of the flow beneath the curved geometry. Momentum driven flows such as that produced by the propane burner generate significantly longer flames than buoyancy driven flows such as those produced by the heptane pool fires. Taking this into account, for the curved ceiling setup the flame lengths obtained when the fire is flush to the sidewall were the longest using the propane burner. Adaptations of the correlations were obtained thanks to linear regression of the test results and show a better relationship between the different burner positions and fuel types. While these correlations show better representation of the test data compared to the existing ones, execution of additional tests and research would provide improved and more general models.

The temperature distribution inside the setup during the tests was also investi-

gated. Temperatures were measured using K-Type thermocouples at various points, and the results revealed that temperatures were higher at the fire's impingement point and reduced as the flame moved away from it. Additionally, the propane fires produced higher temperatures than the heptane fires did, and the higher propane flow fire was linked to higher temperature values. While the results that were found provide good insight into the temperature development within the setups, the use of more thermocouples could have resulted in more precise readings. This could provide a more detailed understanding of the correlation between temperature and the flame's lenght, if there is one. Furthermore, the utilization of new thermocouples could have resulted in more accurate readings than the ones found during the tests.

Chapter 10

Conclusion

- Thanks to an in depth literature research it was determined that literature on the topic of *"Flame Extensions Under Ceilings"* was mainly available for the flat ceiling case. In particular, correlations found by You and Faeth, Gao et Al. and Zhang et Al. were deemed as the most relevant for the work in this project. While fewer compared to the flat ceiling case, the models found by Zhang et Al. and Pan et Al. to represent the flame extensions under curved ceilings were adopted for the comparison with the test data from the experimental results.

- The ceiling geometry was found to play a significant role in the development of flames beneath it. Notably, due to the curvature of the curved ceiling, after impingement flames need to travel longer beneath it in order to fully combust. The curved geometry impacts the buoyancy component of the ceiling jet flow, extending it and consequently producing longer flames compared to the flat ceiling case. Since in the flat ceiling, there is not change in height after impingement, the buoyancy component of the flow does not vary.

- Changes in the heat release rate of the fire result in flame length variations.

In particular, the higher the HRR, the longer the flame extension: this is valid for both flat and curved ceiling geometries, with the curved ceiling producing longer flames than the flat one. Variation of the fuel type also impacts the flame extension beneath the ceiling. A heptane pool fire and propane gas burner were used in the tests. The former produces a buoyancy driven flow during combustion, while the latter is characterized by a momentum driven flow since a gas flow rate needs to be provided to supply the fuel. The momentum component of the gas burner extends the flames beneath the ceiling further than the heptane pool fire which is only driven by buoyancy. This difference is particularly relevant in the curved ceiling setup. Finally, the burners were tested both in the centre each the setup and flush to one of their sidewalls. For heptane, the largest flame lengths are obtained in the centre position in both setups. When placed flush to the setup's sidewall, entrainment is restricted affecting the combustion efficiency, the HRR and consequently the flame extension. In the central position, the fire can burn freely and with increased entrainment resulting in higher HRR and flame lenght values. For propane, the largest flame extensions are found whith the burner positioned flush to the sidewall. Reduced entrainment from in the side position does not affect the combustion efficiency of the momentum driven flow, but makes the flame travel further to undergo full combustion. This results in the longer flames compared to the central position where entrainment is greater and flame extensions are shorter.

- Determination of the correlation between the test results and models and empirical correlations found in literature for flame extensions under ceilings. Comparison between the test data and the models from literature in general shows some dissimilarities. These can be attributed to differences in the test

setups, different fuel types and errors in the recording and analysis of the test videos. While the flat ceiling has been extensively studied in literature, for the curved ceiling a more in depth analysis was performed. In particular, after comparing the test data with literature's flame length models, new adaptations of the existing correlations were developed using linear regression.

Bibliography

[1] NFPA - Deadliest fires or explosions in the world https://www.nfpa.org/News-and-Research/Data-research-and-tools/US-Fire-Problem/Catastrophic-multiple-death-fires/Deadliest-fires-or-explosions-in-the-world

[2] Brian Y. Lattimer, Christopher Mealy and Jesse Beitel, Hughes Associates, Inc. (2012) *Heat Fluxes and Flame Lengths from Fires Under Ceilings*

[3] Fei Tang, Peng Hu, Qing He, Jianping Zhang, Jennifer Wen (2021) *Effect of sidewall on the flame extension characteristics beneath a ceiling induced by carriage fire in a channel*

[4] L. Chen, X. Liu, Y. Lan, S. Zhou, X. Li, X. Yan, H. Chen, *"Experimental study on the smoke movement and flame extension length characteristics of strong fire plumes in a sealed tunnel," Tunnelling and Underground Space Technology 131 (2023) 104780.*

[5] H. Z. You, G. M. Faeth, *"Ceiling heat transfer during fire plume and fire impingement," Fire and Materials, vol. 2, Issue 3, pp. 140-147, 1979.*

[6] H. Ingason. Y. Zhen Li, A. Lönnermark *Tunnel Fire Dynamics - Springer 2015*

[7] Pagnon Eriksson, Claude; Johansson, Nils (2020) *Review of wildfire indices, Indices applicable for a Swedish context*

[8] LUB Search Link https://eds.s.ebscohost.com/eds/search/basic?vid=0&sid=50df0d58-d082-41ee-b4f0-09188fd30dcb%40redis

[9] Säfsten, K., Gustavsson, M. and Ehnsiö, R (2020) *Research methodology: for engineers and other problem-solvers. Studentlitteratur AB*

[10] Morgan J. Hurley *SFPE Handbook of Fire Protection Engineering - Fifth Edition Vol. 1*

[11] G. Heskestad, J. L. De Ris, *"Fire plume correlations", Fire Technology, vol. 12, no. 4, pp. 274-282, 1976*

[12] G. Heskestad, T. Hamada, *"Ceiling Jets of Strong Fire Plumes," Fire Safety Journal, vol. 21, pp. 69-82, 1993.*

[13] G. Heskestad, *"Smoke Filling in Simple Enclosures," Fire Safety Journal, vol. 8, pp. 95-106, 1984.*

[14] P. L. Hinkley, H. G. H. Wraight, C. R. Theobald, *"The Contribution of Flames under Ceilings to Fire Spread in Compartments," Fire Safety Journal, 7 (1984) 227 - 142*

[15] X. Zhang, L. Hu, X. Zhang, *"Flame lengths in two directions underneath a ceiling induced by line-source fire: An experimental study and global model," Proceedings of the Combustion Institute 38 (2021) 4561–4568*

[16] X. Zhang, H. Tao, Z. Zhang, J. Liu, A. Liu, W. Xu, X. Liu, *"Flame extension area of unconfined thermal ceiling jets induced by rectangular-source jet fire impingement," Applied Thermal Engineering 132 (2018) 801–807*

[17] H. Ding, J. G. Quintiere, *"An integral model for turbulent flame radial lengths under a ceiling," Fire Safety Journal 52 (2012) 25–33.*

[18] Z. Zhaoa, Q. Cao, *"The development of urban underground space from the perspective of urban economy," Procedia Engineering 21 (2011) 767 – 770.*

[19] R. Pan, G. Zhu, Z. Liang, G. Zhang, H. Liu, X. Zhou, *"Experimental study on the fire shape and maximum temperature beneath ceiling centerline in utility tunnel under the effect of curved sidewall," Tunnelling and Underground Space Technology 99 (2020) 103304.*

[20] R. Pan, G. Zhu, G. Xu, X Liu, *"Experimental and theoretical analysis on extension flame length of buoyancy-induced fire plume beneath the curved ceiling," Tunnelling and Underground Space Technology 122 (2022) 104365.*

[21] Y. Zhen Li, H. Ingason, *"Model Scale Tunnel Fire Tests – Automatic Sprinkler ," BRANDFORSK project 501-091 (2011).*

[22] Q. Guo, K. J. Root, A. Carlton, S. E. Quiel, C. J. Naito, *"Framework for rapid prediction of fire-induced heat flux on concrete tunnel liners with curved ceilings ," Fire Safety Journal 109 (2019) 102866.*

[23] Biltema, *"Biltema Brandmassa - Product Sheet", https://docs.biltema.com/v2/documents/file/sv/e0d02970-1698-4700-8d2a-cab5281d1c9b .*

[24] R. Pan, G. Zhu, G. Xu, X Liu, *"Experimental and theoretical analysis on extension flame length of buoyancy-induced fire plume beneath the curved ceiling," Tunnelling and Underground Space Technology 122 (2022) 104365.*

[25] Houtwerf, *"Promatect® -H Product Sheet"*, https://www.houtwerf.nl/webshop/uploads/2016/08/Promatec_H_-_2016_-_ENG.pdf .

[26] Lund Universitet, *"Avfallshandbok,"* https://www.medarbetarwebben.lu.se/sites/medarbetarwebben.lu.se/files/avfallshandbok-lu-version1-2016-02-10.pdf *2016.*

[27] D. Madsen, *"Instruktion för hantering av brandfarlig gas vid Avdelningen för Brandteknik; Instruction for the handling of flammable gas at the Division of Fire Safety Engineering," ed: Tillgänglig i pärm för Brandfarlig vara; Available in the folder Brandfarlig vara (English Flammable goods)," 2020.*

[28] D. Madsen, *"Instruktion för hantering av brandfarlig vätska vid Avdelningen för Brandteknik; Instruction for the handling of flammable liquid at the Division of Fire Safety Engineering," ed: Tillgänglig i pärm för Brandfarlig vara; Available in the folder Brandfarlig vara (English: Flammable goods)," 2020.*

[29] Lund University, *"Safety procedures for laborativ and experimental activities at the Department of Fire Safety Engineering,"* .

[30] B. Karlsson, J. G. Quintiere, *"Enclosure Fire Dynamics, Second Edition," (2022).*

[31] R. Li, Z. Liu, Y. Han, M. Tan, Y. Xu, J. Tian, J. Yan, X. Meng, M. Wei, S. Hu, D. Chong, L. Li *"Experimental study of the combustion and emission characteristics of ethanol, diesel-gasoline, n-heptane-iso-octane, n-heptane-ethanol and decane-ethanol in a constant volume vessel," (2018).*

[32] National Center for Biotechnology Information. *"PubChem Compound Summary for CID 6334, Propane. Retrieved April 1, 2023 from* https://www.aqua-calc.com/calculate/weight-to-volume/substance/propane-coma-and-blank-gas*," (2023).*

[33] M.L. Janssens, *"Measuring rate of heat release by oxygen consumption," Fire Technology 27, 234–249 (1991).*

[34] A. Hamins, S. J. Fischer T. Kashiwagi, M. S. Klassen, *"Heat Feedback to the Fuel Surface in Pool Fires," Combustion Science and Technology (1994).*

[35] Open CV *"*https://opencv.org/*"* .

[36] Google Colab *"*https://colab.research.google.com/*"* .

[37] Z. Gao, JieJi, H. Wana, J. Zhua, J. Suna, *"Experimental investigation on transverse ceiling flame length and temperature distribution of sidewall confined tunnel fire," Fire Safety Journal 91 (2017) 371–379.*

[38] J. Wang, G. Cui, X. Kong, K. Lu , X. Jiang, *"Flame height and axial plume temperature profile of bounded fires in aircraft cargo compartment with low-pressure," Case Studies in Thermal Engineering 33 (2022) 101918.*

[39] T. Zhou, Y. Zhou, C. Fan, J. Wang, *"Experimental study on temperature distribution beneath an arced tunnel ceiling with various fire locations," Tunnelling and Underground Space Technology 98 (2020) 103344.*

Appendix

Fire Video Detection Python Code

```
 # import the necessary packages
import cv2
import numpy as np
from IPython.display import clear_output
import matplotlib.pyplot as plt
from skimage import morphology
import math


#video we are going to analyze
cap1 = cv2.VideoCapture('/content/TRIM_P_Ts_T1_04_slow.mp4')

#information regarding the video
frame_count = int(cap1.get(cv2.CAP_PROP_FRAME_COUNT))
print('Frame count: ', frame_count)
print('Frame rate: ', cv2.CAP_PROP_FPS)


# #create video object where we are going to write our results to
frame_width1 = int(cap1.get(3))
frame_height1 = int(cap1.get(4))
frame_size1 = (frame_width1,frame_height1)
fps1 = cv2.CAP_PROP_FPS
print('Frame size: ', frame_size1)


# Define the codec and create VideoWriter object
lenght_output_video1 = cv2.VideoWriter('length_output_video1.avi', cv2.VideoWriter_


frameToStart = 0 #0
cap.set(cv2.CAP_PROP_POS_FRAMES, frameToStart)
```

```
while(cap.isOpened()):
  ret, frame = cap.read()

  #if no frame found or frame is None
  if(not ret or frame is None):
    break


  # Flame detection/counting #

  #HSV color filtering

  frameHSV = cv2.cvtColor(frame, cv2.COLOR_BGR2HSV)

  #define lower/upper range
  lower_orange = np.array([0,0,255])
  upper_orange = np.array([40,170,255]) #GoPro

  #generate masks
  mask = cv2.inRange(frameHSV, lower_orange, upper_orange)

  #generate output image of detected flame pixels
  results=cv2.bitwise_and(frame, frame, mask=mask)
  results_sidebyside=cv2.hconcat([frame, results])

  output_video_sidebyside.write(results_sidebyside)



#when finished 'close' the video objects
cap.release()
output_video.release()


frameToStart = 0
cap1.set(cv2.CAP_PROP_POS_FRAMES, frameToStart)

# Define the conversion factor from pixels to meters
# pixels_to_meters1 = 0.0009769094138543516873898756660746 #normal
pixels_to_meters1 = 0.0012423625254582484725050916496 9 #slow motion

# Initialize the total flame length to 0
total_flame_length1 = 0

# Initialize a list to store the heights of the flames in each frame
heights1 = []
heights_m1 = []
areas1 = []
widths1 = []
widths_m1 = []
avg_LD1 = []
```

```
# Initialize a counter for the number of frames
frame_count1 = 0

# Loop over each frame of the video
while cap1.isOpened():
    # Read the current frame
    ret1, frame1 = cap1.read()

    # If the frame is not valid, break out of the loop
    if not ret1:
        break

    # Convert the frame to grayscale
    gray1 = cv2.cvtColor(frame1, cv2.COLOR_BGR2GRAY)

    # Apply threshold to separate the fire from the background
    # _, thresh1 = cv2.threshold(gray1, 240, 255, cv2.THRESH_BINARY)
    _, thresh1 = cv2.threshold(gray1, 170, 255, cv2.THRESH_BINARY) #slowmotion

    # Use Canny edge detection to find the edges of the flames
    edges1 = cv2.Canny(thresh1, 100, 200)

    # Find the contours of the flames
    contours1, _ = cv2.findContours(edges1, cv2.RETR_EXTERNAL, \\cv2.CHAIN_APPROX_S

    # Initialize the height of the fire to 0
    height1 = 0
    area1=0

    # Initialize the bounding rectangle of the fire to None
    rect1 = None

    # Loop over each contour
    for c1 in contours1:
        # Find the bounding rectangle of the contour
        x1, y1, w1, h1 = cv2.boundingRect(c1)

        # Update the height of the fire
        height1 += h1
        area1=w1*h1

        # Append the height of the fire to the list of heights
        # heights.append(h*pixels_to_meters)
        # heights.append(h)
        areas1.append(area1)
        # widths.append(w)
        LD1=h1/w1
        avg_LD1.append(LD1)

        # If the bounding rectangle is not set, set it to the current rectangle
```

```
        if rect1 is None:
            rect1 = (x1, y1, w1, h1)
        # Otherwise, update the bounding rectangle to include the current rectangle
        else:
            x0, y0, w0, h0 = rect1
            x2, y2 = max(x0, x1), max(y0, y1)
            x3, y3 = min(x0 + w0, x1 + w1), min(y0 + h0, y1 + h1)
            rect1 = (x2, y2, x3 - x2, y3 - y2)


    # If a bounding rectangle was found, draw it on the frame
    if rect1 is not None:
        x1, y1, w1, h1 = rect1
        pic1=cv2.rectangle(frame1, (x1, y1), (x1 + w1, y1 + h1), (0, 0, 255), 2)

        # Add the height of the fire to the total flame length
        total_flame_length1 += height1 * pixels_to_meters1
        # heights.append(height * pixels_to_meters)


        # Increment the frame counter
        frame_count1 += 1

    # write the frame to video
    lenght_output_video1.write(pic1)
    heights1.append(-h1) #heights in pixels, need to determine the height of someth
    heights_m1.append(-h1*pixels_to_meters1)
    widths1.append(-w1)
    widths_m1.append(-w1*pixels_to_meters1)

# Release the video capture
cap1.release()

# Compute the average height of the fire
avg_height1 = sum(heights1) / len(heights1) if heights1 else 0
avg_height_m1 = sum(heights_m1) / len(heights_m1) if heights_m1 else 0
avg_width1 = sum(widths1) / len(widths1) if widths1 else 0
avg_width_m1 = sum(widths_m1) / len(widths_m1) if widths_m1 else 0



# Print the average height of the fire
print("Average height of fire [pix]:", avg_height1)
print("Average height of fire [m]:", avg_height_m1)
print("Average width of fire [pix]:", avg_width1)
print("Average width of fire [m]:", avg_width_m1)

#print results to excel
import pandas as pd
df1=pd.DataFrame({'flame_height':heights_m1, 'flame_width':widths_m1})
print(df1)
```

```
df1.to_excel('TRIM_P_Ts_T3_075_slow_flames.xlsx')#, sheet_name='new_sheet_name')
```